Study on Pressure Responses at Injection and Observation Wells in an Aquifer by CO_2 Geological Storage

孙, 强

Study on Pressure Responses at Injection and Observation Wells in an Aquifer by CO_2 Geological Storage

Sun Qiang

2021

Study on Pressure Responses at Injection and Observation Wells in an Aquifer by CO_2 Geological Storage

A dissertation submitted to Kyushu University

For the degree of Doctor of Engineering

By

Sun Qiang

Supervised by

Prof. Sasaki Kyuro

KYUSHU UNIVERSITY

Department of Earth Resources Engineering

Graduate School of Engineering

Kyushu University

Fukuoka, Japan

March 2021

Abstract

CO_2 capture and geological storage (CCS) is a method of reducing CO_2 emissions into the atmosphere. It is operated by CO_2 capture from large-scale CO_2 emission sources such as power plants. The CO_2 gas is further sequestered into underground reservoirs with relatively high permeability and porosity, such as deep saline aquifers. From the previous and on-going CCS projects, it has been implemented that CCS is technically feasible. For further CCS projects implemented to mitigate global warming and climate change, it is indispensable to establish the safe operation of CO_2 storage and monitoring system of the reservoir and surrounding environment, because it is expected to increase the CO_2 injection rate and cumulative injection amount to promote commercial CCS projects.

In this study, the pressure build-up and fall-off in the CO_2 injection well and the pressure response in the observation well drilled at a distance of 1 to 5 km were investigated by numerical simulations. In particular, the present research objective is to provide design data for the distance of the observation well and the required measurement sensitivity of the pressure transmitter installed in the observation well by clarifying the relationship between the aquifer conditions and the pressure response in the observation well. Furthermore, a prediction method using an approximate analytical solution was also presented to predict them.

This dissertation consists of the following 6 chapters.

Chapter 1 introduces the recent CCS projects in the world and the technological development challenges for monitoring systems related to safe CO_2 geological storage. The focus was directed towards three world-famous CCS commercial projects including the Tomakomai CCS demonstration project (hereinafter Tomakomai CCS project). The aquifer characteristics and differences between them are highlighted. CO_2 geological storage in a deep aquifer is characterized by pressure build-up (PBU), pressure fall-off (PFO), convection flow of CO_2 plume, and pressure propagation in the aquifer. One of the monitoring items carried in the current CCS projects is the pressure

response at an observation well drilled a few kilometers away from the injection well. In the case of Tomakomai CCS, the observation well is located approximately 3 km from the injection well.

Chapter 2 describes the aquifer and injection well modeling for CO_2 storage; all defined in the three-dimensional cylindrical coordinate system. The model was referred to as the Moebetsu Formation mainly targeted by the Tomakomai CCS project. The base model of the aquifer with 1000 m in depth and 40 °C in temperature, layer thickness H=100 m, horizontal permeability k_r=370 md, vertical permeability k_z=37 md, porosity ϕ=30 %, and open boundary at outer radius r_e=10 km was used for the numerical simulation using the multiphase reservoir simulator CMG-STARS™. The block model consists of (1000, 1, 10) grid cells in the coordinate (radius, azimuth, altitude). The vertical injection well radius r_w=0.1 m was set at the aquifer center. As for the Tomakomai CCS project, supercritical CO_2 (10 to 14 MPa, 40 °C) is injected from perforated halls in all wellbore blocks contacting with the aquifer. Specifically, PBU, that is the increase from the initial aquifer pressure (=10 MPa), was controlled less than 4 MPa (the average PBU in Tomakomai CCS is reported as 0.45 MPa). In addition, in the Tomakomai CCS project, 6 sets of CO_2 injection with PBU and PFO were conducted during 6 months just after the beginning of CO_2 storage, so the injection period (100 to 500 days) and two injection schemes with single and multiple PBU and PFO were created to compare the pressure response.

On the other hand, the approximate prediction method, which uses the analytical solution of the linearized one-dimensional unsteady reservoir flow equation obtained by assuming an aquifer with open boundary, uniform permeability, and uniform fluid saturation, was presented to predict rough PBU, PFO, and pressure response at a radial position. It was shown that the main parameters in the solution are permeability-thickness product, $k_r \cdot H$, and hydraulic diffusivity, η.

Chapter 3 is a band for a single scheme that blocks the well after performing CO_2 injection for a certain period (50 to 500 days) at the injection rate q_m=100 to 800 t-CO_2/day in the initial stage of CO_2 underground storage. It describes the CO_2 saturation

distribution in the aquifer and the numerical simulation results for PBU and PFO in the injection well. The increase in PBU is inversely proportional to $k_r \cdot H$. In addition, until the elapsed time t=100 days from the start of CO_2 injection, the radius position of the CO_2 plume front observed at the aquifer top expands in proportion to $t^{1/2}$, and after the shut-in, it gradually expands in proportion to $0.1t$ due to buoyancy force on CO_2. The CO_2 saturation around the injection well increases to about 0.35 with the elapsed time and reduces the effective fluid viscosity. However, the decrease in PBU is about 5% compared to the case of injecting saline water. It is the reason that the CO_2 saturation in the aquifer is limited by the irreducible water saturation of 0.65, and PBU does not decrease significantly even if the CO_2 viscosity is less than 1/10 of water. On the other hand, it was confirmed that the time required to reduce by half the PBU decreases exponentially with increasing η.

Chapter 4 summarizes the numerical simulation results of the pressure response in the observation wells to the CO_2 injection with a single set of PBU and PFO. In particular, the pressure ratio R (=maximum response pressure at the observation well / PBU at the injection well) was obtained against the parameters such as permeability k_r, CO_2 injection rate q, and the location of the observation well, r_m. The pressure ratio value of R does not change significantly with q_m, but it decreases in inverse proportion to r_m. For example, when r_m=3 km, the range of the pressure ratio is estimated to be R=0.07 to 0.12 for the base model based on Moebetsu Formation. It was also shown that the time delay Δt_{max}, which is the time difference between the shut-in time and the time that the maximum pressure response is recorded at the observation well, is also inversely proportional to η and increases in proportion to r_m^2. For instance, when the well distance is r_m=3 km, it was estimated Δt_{max}=2 to 10 days.

In Chapter 5, the numerical simulation results of pressure ratio, R and the time delay, Δt_{max} for multiple scheme (6 sets of CO_2 injection with PBU and PFO), as shown in the initial stage of the Tomakomai CCS project, are compared with the single CO_2 injection scheme. It was revealed that R gradually increases with each repetition of multiple CO_2 injections, but Δt_{max} does not show any difference between single and multiple schemes.

Finally, when the pressure response at the observation well is used to estimate the aquifer condition based on the numerical simulation results, it was shown that the observation well location and the minimum sensitivity of the pressure transmitter installed are important design factors for the observation well function. For example, in the case of the observation well distance is equal to r_m=3 km, the minimum sensitivity of the pressure transmitter needs approximately 1 kPa order under the absolute pressure (or pressure resistance) of 10 to 11 MPa to obtain an accuracy of 2 digits. However, in the case in an event in which the minimum sensitivity is 10 kPa order, the well distance required should be lesser than, r_m=1 km.

Chapter 6 summarizes the conclusions of this thesis and also explains future research topics.

Table of Contents

List of Tables

List of Figures

Acknowledgments

I sincerely express my deep sense of gratitude to Professor Kyuro Sasaki for his extraordinary cooperation, invaluable guidance, and supervision. His advice and encouragement polish my critical thinking and lead me toward an independent researcher. I owe and respectfully offer my thanks to Professor Yuichi Sugai, and Assistant Professor Ronald Nguele for their kind supports, valuable suggestions, and useful comments throughout this research work.

I would like to show my deep gratitude and appreciation to Associate Professor Hirokazu Okawa for his critical reviews and comments on my dissertation.

I gratefully acknowledge the financial support received from the Japanese Government (MEXT) to pursue my Ph.D. study at Kyushu University. I also want to say thanks for the China Scholarship Council (CSC) for they give me a chance to apply for the MEXT Scholarship.

I cherish every moment I spent with my colleagues of the Resources Production and Safety Engineering Laboratory for their support and kind assistance. Our friendship will last long even we graduate and separate.

I would like to thank my mother, my wife, my son, and my sisters for their selfless support and understanding. Finally, I want to say thanks to my son, your smile always calms me down and gives me faith and motivation to overcome challenges.

Chapter 1: Introduction

1.1 Global warming and CCS (CO_2 capture and geological storage)

Greenhouse gases from human activities are the most significant driver of observed climate changes since the Mid-20th century (Edenhofer and Seyboth, 2013; Kweku et al., 2017; Mikhaylov et al., 2020; Qiao et al., 2019). The concentrations of greenhouse gases such as carbon dioxide (CO_2), methane (CH_4), chlorofluorocarbons (CFCs), et al (Ledley et al., 1999). in the atmosphere are growing faster and faster since the industrial revolution which leads to a more and more serious global warming effect. Among them, CO_2 gas is the main contributor to global warming and climate change which makes up an estimated more than 77% of greenhouse gas (Rahman et al., 2017).

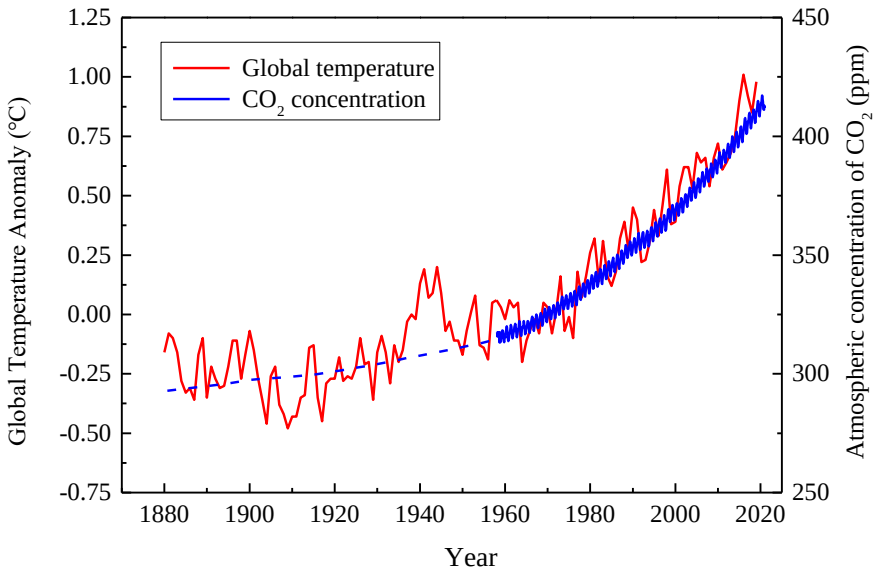

Figure 1-1. Correlation between atmospheric concentration of CO_2 and the global temperature since the 1880s (Humlum et al., 2013)

As is shown in Figure 1-1 the continuous rise in the Earth's surface temperature is strongly linked with the atmospheric CO_2 concentration, which suggests that CO_2 is a significant contributor to global warming and climate change. According to some

statistics (Lake and Lomax, 2019), the average atmospheric CO_2 concentration is increasing continuously by more than 1.5 ppm/year[3]. Under this growth rate in the average atmospheric CO_2 concentration, it will exceed 450 ppm and means the global temperature will exceed a dangerous level of over 2°C than the present one within the next 20 years (Ritchie and Roser, 2020).

To mitigate the increasing rate, many intergovernmental organizations have worked to assess climate change, exchange technology, and experience of reducing anthropogenic CO_2 emissions (IEACHG, 2010; Metz et al., 2005; Shackley et al., 2005). In 2017, a possible frame to reduce CO_2 emissions into the atmosphere has been agreed upon among countries that joined COP23 (Obergassel et al., 2018). The CO_2 concentration in the atmosphere could be controlled either by reducing its production releasing it into the atmosphere or by capturing and storing CO_2 in a safe place for a long time. Nowadays, fossil resources are still the domination of the energy supply (86% of the global energy supplements in 2017), which means it is difficult to cut a large amount of CO_2 emission by reducing its production in a short period. Even though the new energy industry is developing rapidly, it is not yet capable of making a decisive contribution to the replacement of fossil energy to reduce CO_2 emissions in a short and medium period.

CO_2 capture and geological storage (CCS) provides a promising way to mitigate CO_2 emissions into the atmosphere by capturing CO_2 gases from relatively large industrial sources, such as power plants, transporting and injecting them into porous and permeable storage reservoirs[3]. The International Energy Agency (IEA) has estimated the potential contribution of CCS in mitigation of climate change to be as high as 20 % of the global emissions in 2050 and is second only to improvement in energy efficiency (Goel, 2012). And they also make the Blue Map reduction plan that it is needed to continue annual geological storage of 9.5 Gt-CO_2 by CCS for 45 years. Therefore, multiple measures are needed to deal with the more and more serious climate change and global warming to transition the situation of fossil fuel exhaustion.

1.2 CO_2 properties in reservoir condition and pressure build-up induced by CO_2 injection

1.2.1 CO_2 properties in reservoir condition

Three main underground storage reservoirs have been identified: saline aquifers, depleted oil and gas reservoirs, and unminable coal seams (Yang et al., 2010). Deep saline aquifers have been considered as ideal storage sites because of the large storage capacity and broad distribution worldwide.

The saline aquifers are geologic layers of permeable rock that are located 1,000 to 3,000 m undersurfaces (Zhang and Huisingh, 2017) which can ensure injected CO_2 in a supercritical state (P_c>7.39 MPa, T_c>31.26℃) at the reservoir conditions. These aquifers are saturated with high-salinity brine water, which is difficult to utilize directly, however, can be used as suitable storage sites for CO_2.

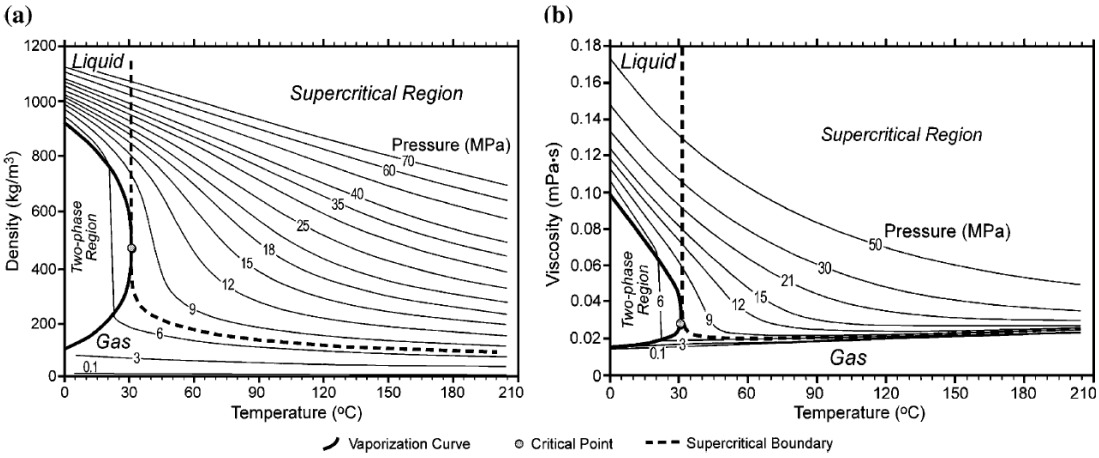

Figure 1-2. Density and viscosity value of CO_2 (Nordbotten et al., 2005)

The density and viscosity value for CO_2 is shown in Figure 1-2. CO_2 is in a supercritical state (Hereinafter $scCO_2$) in the reservoir condition with a large density (150-800 kg/m^3) and viscosity (0.023×10^{-6}-0.0611×10^{-6} kPa·s) than it was in a gas state (Nordbotten et al., 2005). However, the density of $scCO_2$ is still smaller than that of saline water (>1000 kg/m^3) which will make the injected CO_2 cumulative below the seal layer under the action of buoyancy force.

1.2.2 Pressure build-up induced by CO_2 injection

Several ongoing pilots and commercial CCS projects have suggested that CO_2 geological storages in deep sedimentary formations are technologically feasible (Eiken et al., 2011; Hansen et al., 2013; Tanaka et al., 2014). However, the CO_2 reduction rate by CCS projects is limited at present because enough CCS projects have not been implemented by economical and safety issues that are related to social acceptance (Romasheva and Ilinova, 2019). Most of the existing CCS projects are on a pilot scale for the purpose of obtaining experience for future commercial-scale CCS projects, which is not enough to store a large amount of CO_2. According to the existing CCS project monitoring data and some theoretical and numerical studies (Rutqvist, 2012), to make a significant contribution to the mitigation of climate change, many commercial CCS projects with larger CO_2 injection rates from an injection well need to be planned and implemented. The pressure build-up induced by CO_2 injection may be a threshold to limit the single-well injection rate and the safety of storage. Thus, studying the injection-induced pressure build-up, the integrity of the seal layer is the key point to make sure the stability and safety of sequestered CO_2 (Shukla et al., 2010).

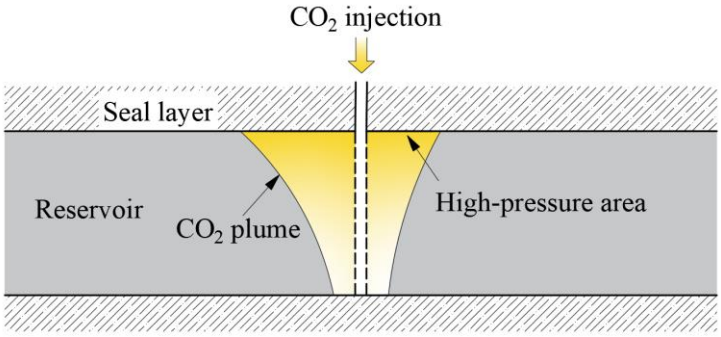

Figure 1-3. Schematic of pressure build-up induced by CO_2 injection

A suitable CO_2 storage site should have a relatively large permeability and porosity to store a large amount of CO_2. Above the reservoir is a top seal layer as a flow barrier with a permeability far less than the reservoirs to stop the stored CO_2 from leaking to the surface or sea bottom, like unfaulted clays, claystones, mudstones, or salt beds.

Ideally, the caprock could be plastic, having a high capillary entry pressure and homogenous over a large lateral distance (Rutqvist, 2012). During injection, the CO_2 injection-induced pressure elevate in the reservoir from its original geomechanical pressure. Because of the buoyance force, the injected CO_2 accumulates below the seal layer which may result in a high-pressure concentration around the seal layer, and high-pressure build-up will provide a large risk to the seal layer which may damage the seal layer and lead to the leakage of CO_2 (Gao et al., 2014; Meckel et al., 2013; Pourtoy et al., 2013). Figure 1-3 shows the schematic of pressure build-up induced by CO_2 injection, high pressure will accumulate in the vicinity of the injection well. If the BHP overpressure exceeds the capillary entry pressure, the caprock will be broken and act as a permeability channel for the CO_2 to diffuse to the up-layers.

1.3 Review of the pressure build-up and fall-off studies

Most of the studies based on CCS are simulation studies to reproduce the performance of the storage reservoir and build-up models to fit the field observational data and make an estimate of the pressure build-up and CO_2 plume front. (Heath et al., 2014) (Khan et al., 2020; Zhang et al., 2016b) studied the impact of boundary conditions and brine extraction on geologic CO_2 storage efficiency and pressure build-up. Using numerical simulation to study investigates storage efficiency of multiwell CO_2 injection and estimate the risks of CO_2 storage. A lot of factors will influence the pressure build-up. (Oruganti and Bryant, 2009) run a simulation study of pressure build-up during CO_2 storage in partially confined aquifers using the simulator CMG STARS. And conclude that the variation of fluid viscosity with pressure and temperature is the dominant effect on injectivity and pressure build-up. (Mathias et al., 2011) studied the pressure build-up during CO_2 injection into a closed brine aquifer and estimated the storage capacity of geological reservoirs for CO_2 storage. (Wu et al., 2018) derived a new governing equation based on the continuity equation that gives an advanced analytical solution about the evolution of fluid pressure with focusing on the role of fluid compressibility. (Vilarrasa et al., 2010) studied the effect

of CO_2 compressibility on CO_2 storage in deep saline aquifers. And find that the error in the interface position caused by neglecting CO_2 compressibility is relatively small when viscous forces dominate, while it can become significant when gravity forces dominate, which is likely to occur at late times of injection. (Joshi et al., 2016) has build-up a simulation model to study the pressure evolution during multiple-wells injection CO_2 in saline aquifers. (Cihan et al., 2013) presented the developed analytical solution for pressure build-up and leakage rate in a multilayered aquifer-aquitard system. (Ashraf, 2014) studies how heterogeneity variation over 160 geological realizations influences the pressure behavior of a typical CO_2 injection operation. (Grude et al., 2014) studied the pressure effect caused by CO_2 injection in the Tubåen formation, the Snøhvit field. And analyzing the salt precipitation on pressure build-up by reducing the porosity and permeability. (Benisch and Bauer, 2013) studied the short and long-term regional pressure build-up during CO_2 injection. And demonstrates that the maximum leakage risk in the caprock may occur significantly after the injection period, not at the end of the injection. (Zhou and Birkholzer, 2011) studied the scale and magnitude of pressure build-up and brine migration induced by large-scale geologic storage of CO_2. (Kim et al., 2011) run the numerical simulation to study pressure evolution from CO_2 injection in saline aquifers effect by salt-precipitation on reservoir permeability, porosity, residual gas saturation et al.

Few researches focus on the pressure fall-off by injecting CO_2. Most of them are estimating the reservoir conditions by analyzing the pressure fall-off data. (Otake, 2013) evaluated the CO_2 distribution underground from the injector's time-lapse pressure fall-off analysis. (Grude et al., 2014) detected a low permeability zone in the Tubåen Formation at the Snøhvit field through analyzing the fall-off pressure data. (Ehlig-Economides et al., 2010) highlight the significance of pressure fall-off tests into the real-time movement of saturation fronts and mobility behavior in the aquifer.

Some researches focused on estimating the reservoir CO_2 storage capacity and

injectivity. (Smith et al., 2011) investigated the impact of boundary conditions on pressure build-up and estimate the CO_2 storage capacity. (Wu et al., 2016) derived an explicit solution for the pressure build-up during CO_2 injection into infinite saline aquifers to obtain the pressure of the reservoir and evaluate the injectivity and safety of reservoirs. (Thibeau et al., 2014) used pressure and volumetric approaches to estimate CO_2 storage capacity in deep saline aquifers with the extraction of water for pressure maintenance. (Gasda et al., 2017) has investigated the pressure-limited storage capacity of the Utsira Formation in the Sleipner CCS project and find that the Utsira can withstand injection rates over 100 Mt/y for 50 years, which is equivalent to 8.3 Gt of CO_2. (Mathias et al., 2009a, b) presents a simple methodology for estimating pressure build-up and screening and selection of sites for CO_2 sequestration.

Nowadays, more and more researchers are focus on how to decrease the pressure build-up. (Singh, 2018) investigated four different injection schemes and compared the injection-induced pressure build-up, the results show that a step-wise injection scheme can prevent a high-pressure build-up. (Fujita et al., 2017) conducted a simulation study based on the Tomakomai CCS project to evaluate the effectiveness of mitigating the pressure build-up by producing the formation water before and during the injection. And think it was a method to increase the effective capacity of injectable CO_2. (Kim and Shin, 2019) also, think about reducing the pressure build-up by producing the formation water. And a dual tubing CO_2-water production horizontal well was considered by a simulation study. The CO_2 is injected at the heel of the horizontal well while the formation water is produced at the toe.

1.4 Monitoring system for CCS

Generally, to confirm that the injected and stored CO_2 is in safe and stable condition, it is necessary to grasp the behavior of CO_2 in the reservoir and to detect whether there is leakage of CO_2 out of the reservoirs or not (Tanaka et al., 2014).

There are a lot of monitoring items to grasp the condition of the geological formations,

pressure and temperature changes, the integrity of formation, and CO_2 saturation and plume performance, et al.. Typically, Table 1-1 shows the monitoring items of the Tomakomai CCS project (Tanaka et al., 2014), five continuous monitoring items, and three periodic monitoring items are in operation. The continuous monitoring items are temperature and pressure in two injection wells, temperature and pressure changes in two remoted observation wells, and seismic monitoring at ocean bottom and onshore, while the periodic monitoring items are marine environmental observation (seawater, bottom mad, and sea lives) and 2D and 3D seismic surveys. Especially, two observation wells were drilled from onshore to Moebetsu Formation (1100-1200 m below) and Takinoue formation (2400-3,000 m below) to record continuous passive changes in aquifer pressure, temperature, and CO_2 saturation in each formation. Those monitoring data recorded in the observation wells can be used to detect the movement of CO_2 plume and judge the stability of stored CO_2 based on comparisons with the numerical simulation results using the aquifer models.

Table 1-1. Monitoring items for Tomakomai CCS project (Tanaka et al., 2014)

Items	Observed objects	Observation frequency
Injection well	1. Downhole: temperature and pressure 2. Wellhead: pressure, injection rate of CO_2	Continuous
Observation well	1. Downhole: temperature and pressure, micro-seismicity, and natural earthquakes	Continuous
OBC: ocean bottom cable	1. Micro-seismicity and natural earthquakes 2. Signal of 2D seismic survey	Continuous
OBS: ocean bottom seismometer	Micro-seismicity and natural earthquakes	Continuous
Onshore seismometer	Micro-seismicity and natural earthquakes	Continuous
2D seismic survey	Distribution of CO_2	Periodic
3D seismic survey	Distribution of CO_2	Periodic

Marine environmental monitoring	Chemical, physical, and biological data	Periodic

1.5 Three commercial CCS projects and the Tomakomai CCS project

1.5.1 In Salah CCS project

The In Salah CCS project started injection CO_2 into Krechba Formation located a 1.9 km deep Carboniferous sandstone unit in 2004. Two horizontal CO_2 injection wells (KB-502 and KB-503) were used to inject CO_2 into the depleted gas reservoir. One abandoned test well in the area (KB-5) was used to detect the CO_2 plume, and the vertical microseismic monitoring well (KB-601) The permeability of the reservoir is only 1.3×10^{-14} m^2 (13 md) and the porosity is about 0.17. The thickness of the reservoir is about 20 m. Figure 1-4 shows the In Salah CCS project and the surface deformation induced by the CO_2 injection. Over the first few years of injection, the InSAR data showed an uplift rate on the order of 5 mm/year above active CO_2 injection wells (Goertz-Allmann et al., 2014; Rutqvist et al., 2010). The background colour indicates the observed surface deformation due to CO_2 injection (data obtained from Tele-Rilevamento Europa TRE). The red box shows the region of interest.

There were few BHP data reported, however, the estimated flowing BHPs are around 29 MPa (based on extrapolation from surface data), considerably higher than the initial formation pressure 18-19 MPa. The maximum pressure increase of about 10-11 MPa above the ambient initial formation pressure has exceeded the fracturing gradient (Rutqvist, 2012; Tanaka et al., 2014). The In Salah CCS project in Algeria has shown significant geomechanical changes because of the injection pressure and site-specific geomechanical conditions. Despite the injection rate of the In Salah CCS project was just 1-1.2 Mt/year, it was still shut down in June 2011 due to concerns about the integrity of the seal layers (Eiken et al., 2011; Verdon et al., 2013).

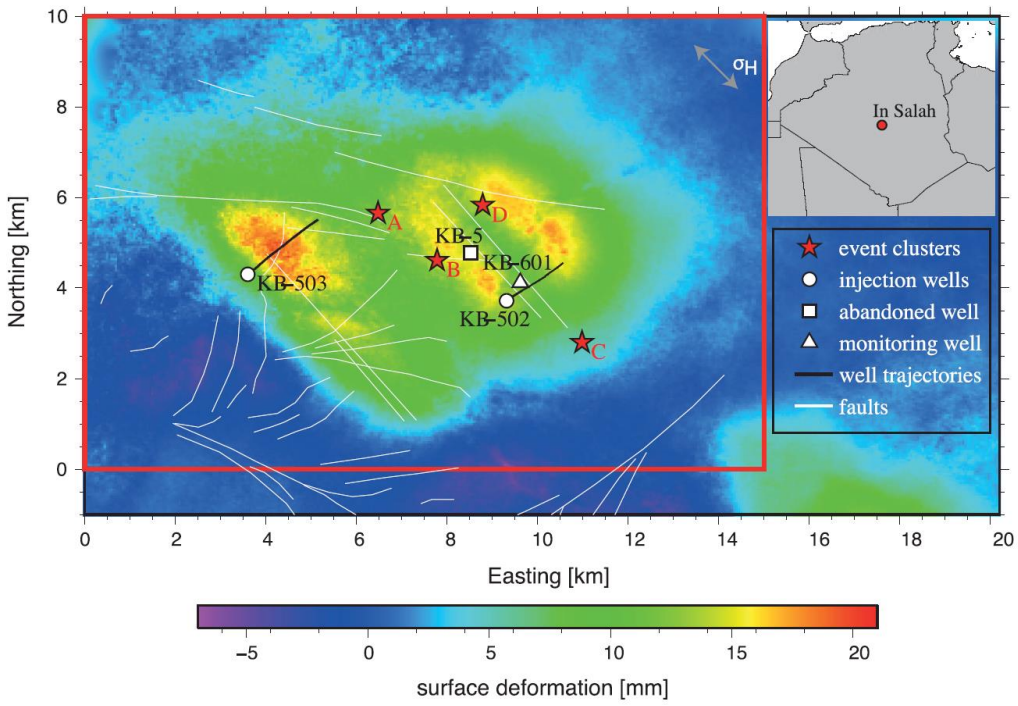

Figure 1-4. Krechba Formation, In Salah, Algeria showing the location of two horizontal CO_2 injection wells (KB-502 and KB-503), one abandoned test well in the area (KB-5), and the vertical microseismic monitoring well (KB-601). (Goertz-Allmann et al., 2014)

1.5.2 Snøhvit CCS project

In the Tubåen Formation at the Snøhvit field Norway (offshore CCS project), Statoil successfully injected 1,600,000 tons of CO_2 from April 2008 to April 2011 with a maximum injection rate of 0.7 Mt/year. It is another CCS program that extracts the CO_2 gas from the gas production well and injection into the underground formation. The reservoir cross-section at Snøhvit is shown in Figure 1-5.

Saline Tubåen Sandstone Formation reservoirs at 2.6 km below the sea bed. The thickness of the Tubåen Formation is about 45-75 m and the permeability of the reservoir was estimated at $0.1\text{-}8\times10^{-13}$ m^2 (10-800 md). The sandstone porosity ranges from 0.07-0.20.

Even though the reservoir permeabilities are larger than fracturing gradient have been measured from cores, the effective permeability of the Tubåen Formation units

around the injection well (F2-H) are much lower than the core data. The lateral extent of such good sands is uncertain, and it was considered as a closed reservoir that is easy to make a high-pressure build-up. The initial pressure is 28 MPa, and the threshold fracture pressure of the seal layer is estimated as 38.8 MPa. Maximum bottom-hole pressure of 39 MPa that been monitored for the Tubåen storage site. It had to stop the CO_2 injection due to a huge increase in bottom hole pressure before reaching the full storage capacity of the Tubåen Formation (Hansen et al., 2013).

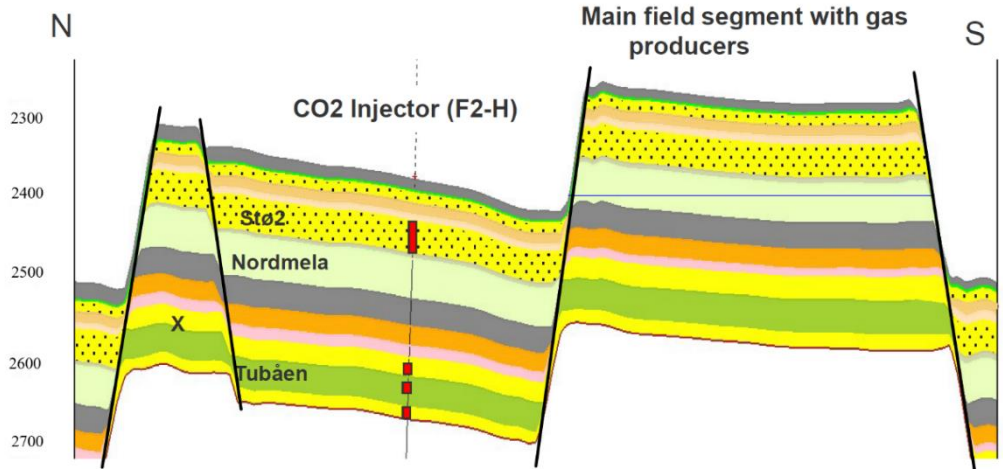

Figure 1-5. Geological cross-section N-S through the reservoir section at Snøhvit (the red dots indicate perforation locations in Tubåen) (Hansen et al., 2013)

1.5.3 Sleipner CCS project

The Sleipner CO_2 storage project of North-Sea, Norway is considered the world's first industrial-scale CO_2 injection project designed specifically as a greenhouse gas mitigation measure. The CO_2 is injected into the Utsira Formation that a deep saline reservoir 800-1,000 m below the sea bed with a range of thickness 200-250 m. The porosities of the Utsira Formation are 0.35-0.40 and permeabilities above 1×10^{-12} m^2 (1000 md). Over 16 million tonnes of CO_2 have been injected since the project started, no significant geomechanical changes have been detected with a maximum injection rate of 0.9 Mt/year (Alnes et al., 2011; Cavanagh and Haszeldine, 2014; Gaus et al., 2005). the pressure build-up induced by CO_2 injection is very small even with a higher single-well injection rate. Figure 1-6 shows the repeated seismic section of the

Sleipner by (Furre et al., 2015). The injected CO_2 is successfully stored in the saline aquifer and accumulated below the seal layer, with almost no leakage to the up-layer. The bottom hole pressure was not measured, but the stable injection and 4D seismic images suggested only a small pressure build-up in the reservoir (Eiken et al., 2011) that far from the threshold pressure.

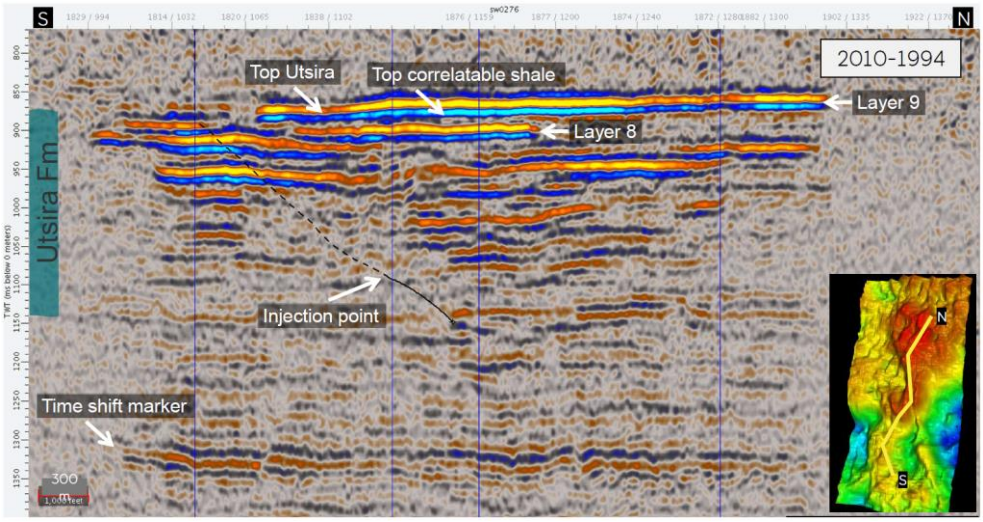

Figure 1-6. Seismic section N-S at Sleipner (Furre et al., 2015; Ringrose et al., 2020)

It is clear that abounded aquifer with small permeability is easier to induce a large pressure build-up and the injection rate of a single injection well will also be limited by the integrity of the formations especially the seal layers. Besides, the heterogeneity of the aquifer will also have great influences on the pressure build-up and evolution in the reservoir.

1.5.4 Tomakomai CCS project

The Tomakomai CCS project of Japan is a large-scale CCS demonstration project as established in 2008 and started injection in 2016. Two horizontal injection wells were drilled from onshore to Moebetsu Formation (1,000-1,200 m below the sea bed) and Takinoue Formation (2,400-3,000 m below the sea bed). The Takinoue Formation was estimated to have a porosity of 0.20-0.40 and permeability of 9-25 md (Tanaka et al., 2017). However, this analysis has overestimated the permeability and the injectivity is far smaller than the initial estimation (nano darcy order in permeability)

(Sawada et al., 2018). For the Moebetsu Formation, it was estimated to have a porosity of 0.03 to 0.19 and permeability of 0.01 md to 7 md before injection. The brine injection test immediately following the drilling and completion of IW-2 indicated that the injectivity of the Moebetsu Formation was very high (hundreds millidarcy order in permeability).

The testing CO_2 injection into the Moebetsu Formation was conducted between April 6th and May 24th, 2016 with 180 to 600 t-CO_2/day in injection rate and 7,163 t-CO_2 in cumulative amount (Sato and Horne, 2018). The threshold pressure was set at 14 MPa. The initial Moebetsu Formation pressure at the injection well was 9.3 MPa and the maximum bottom hole pressure in the injection well was recorded during the test injection was 10 MPa at the maximum injection rate of 0.216 Mt/year and cumulative CO_2 injection was around 0.3 Mt-CO_2 during 4 years injection (Sawada et al., 2018; Tanaka et al., 2017).

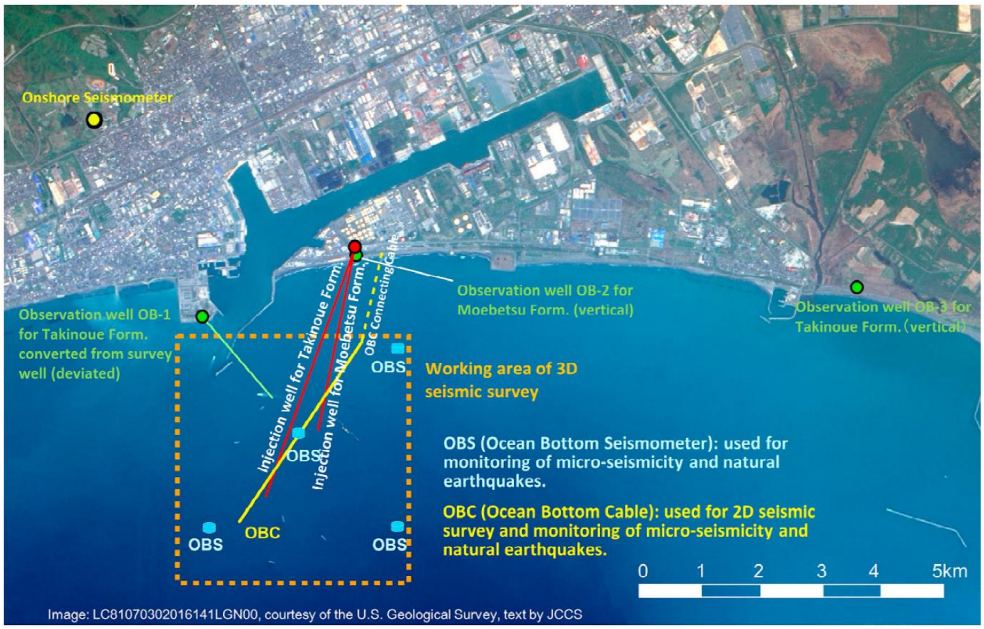

Figure 1-7. Layout of the Tomakomai CCS project monitoring facilities

Figure 1-7 shows the Tomakomai CCS project monitoring items. Two observation wells were drilled to record continuous passive changes in aquifer pressure and temperature and CO_2 saturation in each formation. An observation well OB-2 was

planned (Tanaka et al., 2014) which was drilled 3 km from the injection well in Moebetsu Formation with installing pressure and temperature transmitters.

However, there is no pressure response recorded in the At present, the reason for the no-pressure response at the observation well was explained as the sensitivity of the pressure transducer is not sufficient to detect the pressure propagation from the injection well to the observation well.

1.6 Bottom hole pressure monitoring and observation well

1.6.1 Bottom hole pressure monitoring

Pressure monitoring is one of the continuous monitoring items. The monitoring of bottom hole pressure can provide real-time feedback on the reservoir situation and the integrity of the seal layer. It can be seen in Figure 1-8, the temperature and pressure sensors and downhole seismic sensors were installed in the bottom hole of the CO_2 injection well. to monitor the bottom hole pressure (Finley et al., 2013; Kelley et al., 2014; Meckel et al., 2013; Zhong et al., 2019), temperature (Tao et al., 2013; Zhang et al., 2016a), and the microseismic response (Stork et al., 2015) continuously.

As has been shown in Table 1-1, an observation well drilled with a large distance from the injection well to detect the pressure response induced by CO_2 injection is also another method to grasp the reservoir condition, for instance, the hydraulic conductivity and the leakage or not of the injected CO_2. It can be seen in Figure 1-8, observation well is drilled far from the injection well to permit the observation of subsurface conditions. Temperature and pressure gauges are also installed in the bottom hole for continuous monitoring.

If the distance from observation wells to the injection well is too small, it can indeed be used to detect the CO_2 plume front development. However, according to some *in situ* experience, the greatest risk of CO_2 leakage for any geological storage project is associated with old wells and observation wells (Mathieson et al., 2010). Thus, an

observation well with a small distance to the injection well also creates a new potential pathway for CO_2 leakage to the sublayers which will limit the CO_2 injectivity. Furthermore, drilling a new observation well needs an additional budget and it may create a new potential pathway for CO_2 leakage to the surface. Therefore, the observation well and installed sensors, such as distance from a CO_2 injection well and the sensor sensitivity, should be well-designed before drilling an observation well.

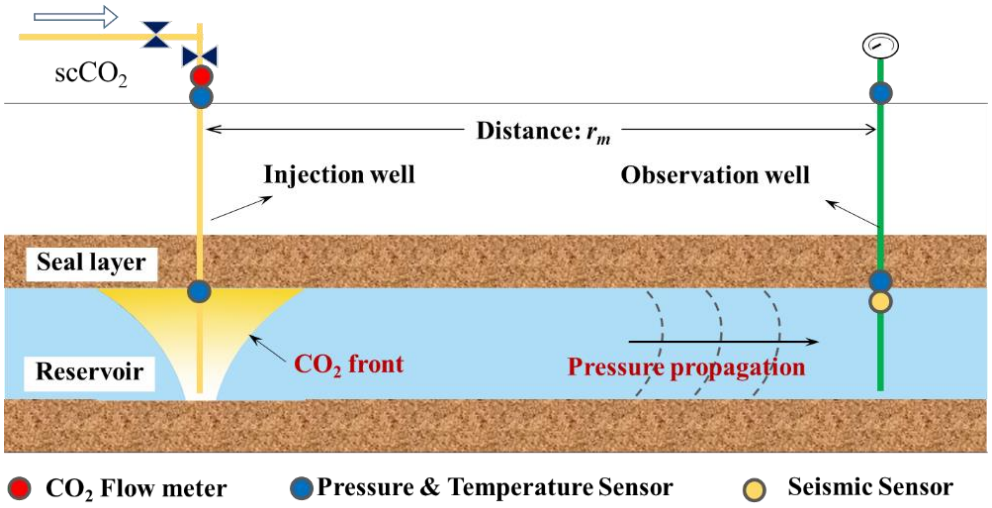

Figure 1-8. Pressure monitoring in the injection well and observation well

1.6.2 Observation well for detecting the reservoir pressure response

The current observation wells for the CCS projects are mainly drilled to grape the CO_2 plume front position (Hosseini et al., 2018; Hu et al., 2015; Mathieson et al., 2011; Mathieson et al., 2010). Because the pressure response of observation well is very small, few researches focus on the pressure response of observation well. However, the monitoring depending on the observation well is also an effective monitoring means, and those monitoring data recorded in the observation wells can be used to detect the movement of CO_2 plume and judge the hydraulic properties of the reservoir based on comparisons with the BHP of injection well. Nowadays few CO_2 storage programs and researches focus on the pressure response of observation well. In this study, the monitoring system between the injection well and observation well was studied to design a reasonable observation well. This can give us another

choice to estimate the hydraulic properties of the reservoir and the safety of sequestered CO_2. In the following, observation wells in the current two CCS projects were introduced briefly.

The In Salah CCS program used an observation well KB-5 (Figure 1-4) (Durucan et al., 2011; Stork et al., 2015) with a distance of 1.3 km from the injection well KB-502 by analyzing the gas tracer injected together with CO_2 to gain the CO_2 plume development. The observation well KB-5 was used for detecting CO_2 plume position not for the pressure analyzing and it was abandoned gas production well drilled in 1980 not well designed for the CCS program.

A Ketzin pilot CCS program in Germany used two observation wells (Ktzi 200 and Ktzi 202) to detect the pressure evolution during injection operation with a distance of 50 m and 112 m from injection well Ktzi 201 (Max. injection rate 0.028 Mt-CO_2/year) respectively (Liebscher et al., 2013; Prevedel et al., 2014; Wiese et al., 2013). The porosity of the reservoir was estimated as 0.13-0.26 by core test and the experimental measurements and NMR data on core samples and in site hydraulic testing indicate permeabilities around 1×10^{-13} m^2 (100 md). The pressure build-up of the injection well was about 1.1-1.7 MPa, while the magnitude of pressure response at observation wells was recorded about 0.4-1.0 MPa with the varying injection rates and several shut-in phases.

1.7 Objectives of study and the outline of chapters

1.7.1 Objectives of the present study

In this study, the pressure monitoring system with an observation well against the pressure build-up was the focus. Even the Tomakomai CCS project drilled an observation well without test and verification before drilling. It gives us an idea to build-up a monitoring system that combined both the pressure in the injection well and the pressure in an observation well. Combined with the Tomakomai CCS project to study the possibility of drilling an observation well that is far from the injection

well (>1000 m) by investigating relations between pressure response at an observation well induced by CO_2 injection in the early stage of CO_2 geological storage in a deep saline aquifer. A criterion to select a pressure transducer installed at an observation well to monitor the pressure responses with sufficient accuracy and resolutions versus the location distances from the injection well and the pressure build-up at the injection well will be discussed. The results can be used as reference data for design an observation well location and installed sensors (or transmitters).

1.7.2 Outline of chapters

Chapter 1: introduces the recent CCS projects in the world and the technological development challenges for monitoring systems related to safe CO_2 geological storage. The aquifer characteristics and pressure build-up induced by injection CO_2 between three world-famous CCS commercial projects including the Tomakomai CCS project are reviewed. The monitoring of reservoir pressure was introduced. One of the monitoring items carried in the current CCS projects, the pressure response at an observation well drilled a few kilometers away from the injection well is highlighted.

Chapter 2: describes the aquifer and injection well modeling for CO_2 storage. A three-dimensional cylindrical model was constructed base on the hydraulic properties of the Moebetsu Formation mainly targeted by Tomakomai CCS project. Two injection schemes with single and multiple PBU and PFO were created to compare the pressure response. The approximate prediction method, that uses the analytical solution of the linearized one-dimensional unsteady reservoir flow equation obtained by assuming open boundary, uniform permeability, and uniform fluid saturation, was presented to predict rough PBU, PFO, and pressure response at a radial position.

Chapter 3: is a band for a single scheme that blocks the well after performing CO_2 injection for a certain period (50 to 500 days) at the injection rate q_m= 100 to 800 t-CO_2/day in the initial stage of CO_2 underground storage. It describes the CO_2 saturation distribution in the aquifer and the numerical simulation results for PBU

and PFO in the injection well.

Chapter 4: summarizes the numerical simulation results of the pressure response in the observation well to the CO_2 injection with a single set of PBU and PFO. In particular, the pressure ratio R (=Max. response pressure at the observation well /PBU at the injection well) was obtained against the parameters such as permeability k_r, CO_2 injection rate q_m, and the location of the observation well, r_m.

Chapter 5: the numerical simulation results of pressure ratio, R and the time delay, Δt_{max} for multiple-injection scheme (6 sets of CO_2 injection with PBU and PFO), as shown in the initial stage of Tomakomai CCS project, are compared with the single CO_2 injection scheme.

Chapter 6: summarizes the conclusions of this thesis and also explains future research topics.

Chapter 2: Numerical simulation model and analysis method

2.1 Aquifer modeling

As shown in Figure 2-1, the three-dimensional cylindrical grid system with (r, φ, z) coordinate was used to construct the reservoir model to simulate pressure and CO_2 saturation distributions by injecting CO_2 from an injection well located at r=0 m into an aquifer with radius r_w. It was assumed that the aquifer has a uniform porosity and permeabilities in horizontal and vertical directions, respectively. Its outer boundary at r=r_e is kept being equal to the initial pressure (open boundary). On the other hand, no-flow across the top and bottom boundaries. The CO_2 plume front position, r_p is defined as a position where CO_2 saturation; S_{CO2}=0.01 that is the minimum detectable CO_2 saturation in present simulations.

Pure CO_2 was injected from the injection well into the aquifer located in the center of the model. The radial distance at a hypothetical observation well from the injection well was defined as r_m. The change of pressure in the aquifer at r=r_m was used as the pressure response at the well bottom of the observation well connects to the aquifer. Numerical simulations were conducted using the compositional reservoir simulator CMG-STARS™.

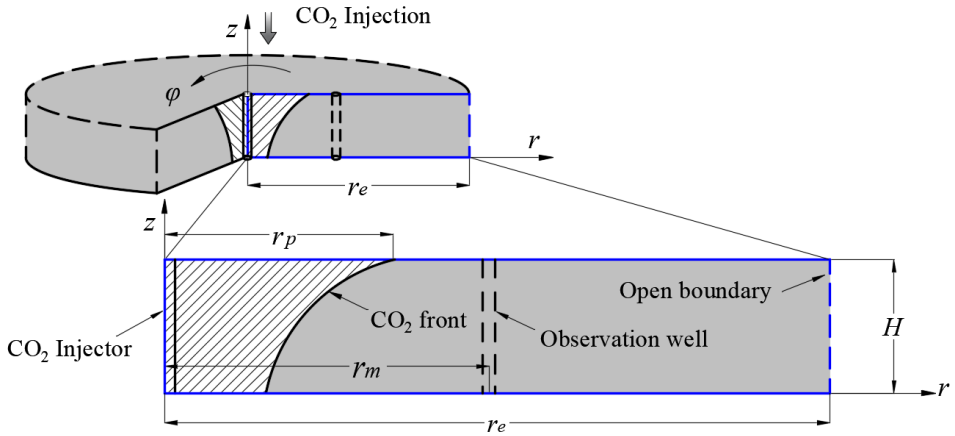

Figure 2-1. Schematic reservoir model

2.2 Numerical simulation system and block model

2.2.1 Block model setting using simulator CMG-STARS™

The simulator CMG STARS (Steam Thermal and Advanced Processes Reservoir simulator) is a new generation reservoir simulator developed by Computer Modeling Group Limited for modeling the flow of three phases, multi-component fluids. CMG STARS can be used to model compositional, steam, geomechanical, dispersed component (polymer, gels, fines, emulsions, and foams) and *in-situ* combustion process. CMG STARS uses a discretized wellbore model which improves modeling by discretizing the wellbore and solving the resulting coupled wellbore and reservoir flow problem simultaneously. The adaptive implicit mode in CMG STARS decides from time-step to time-step which blocks must be solved in implicit or explicit modes.

There are two types of gridding in the CMG STARS, namely rectangular Cartesian grid and radial-angular grid. In this simulation study, the radial-angular grid was used. Since the grid number of the CMG STARS is limited, and it should be less than 10,000 grids. In this simulation study, A typical aquifer model was set by setting r_w=0.1 m and r_e=10 km. The grid-blocks consist of 1,000×1×10 grid cells in the coordinate (radius, azimuth, altitude) directions. The 200 grid-cells between r=0.1 to 400 m, 800 grid-cells between r=400 to 10,000 m were set in the simulation model. The reservoir consists of 10 layers with a constant spacing of 10 m in the vertical direction. The radial distance at a hypothetical observation well from the injection well, r_m was assumed to be a range of r_m=1,000 to 5,000 m. The meshing of the aquifer region in r and z directions is shown in Figure 2-2 and the simplified numerical grid blocks model is shown in Figure 2-3.

For this homogeneous model, off-take at the outer boundary of the model is simulated using a production well and the block was defined as a high permeability (10,000 md). The production well is used to maintain the reservoir pressure constant by setting a BHP constraint as the same as initial pressure.

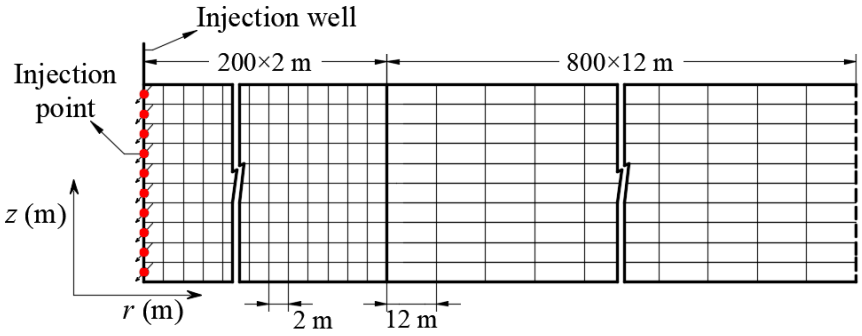

Figure 2-2. Schematic diagram of meshing in the vertical section

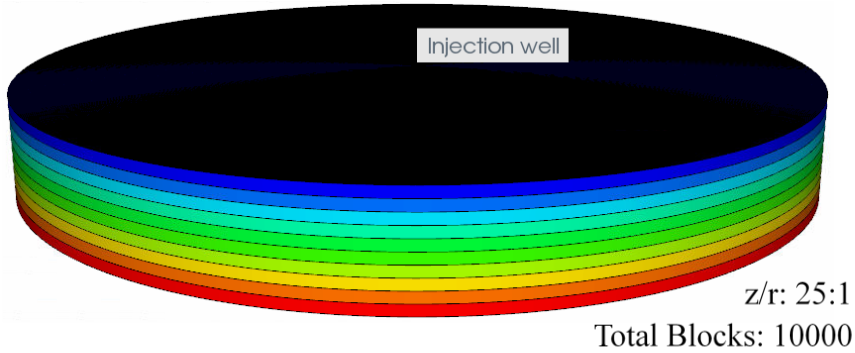

Figure 2-3. Simplified numerical grid blocks model in 3D view

2.2.2 Component Properties

The aquifer was assumed to be composed of two components namely brine and CO_2. CO_2 was defined as gas although it is in a supercritical phase in the reservoir condition. Table 2-1 shows the summary of the physical properties of these two components used in the base model. In the CMG-STARS, the definition of the fluid component viscosity uses the correlation below:

$$\mu = a \cdot e^{b/T} \tag{2-1}$$

Where a and b are coefficients that should be defined in the simulator.

The viscosity depends only on temperature. In present simulations, assuming the ground surface temperature was 15 ℃ and geothermal gradient as 2.5 to 2.75 ℃/100 m, the temperature of the targeted aquifer becomes 40 to 42.5 ℃ and the CO_2 injection temperature was specified as 40 ℃. Therefore, the operation of injection

CO_2 was almost equal to be an isothermal injection process. And the viscosity of both CO_2 and brine water will be assumed approximately constant.

Table 2-1. Summary of the component properties

Component	Brine	CO_2
Molecular weight (kg/gmole)	0.018015	0.04401
Critical pressure (kPa)	22048	7376
Critical temperature (°C)	374.15	31.05
Density (kg/m^3)	1030	600
Viscosity (kPa·s)	6×10^{-7}	0.429×10^{-7}

2.2.3 Rock Fluid Data

Only one rock type is defined for the aquifer, sandstone. Using the default wettability of water-wet. In this model, the formation is an aquifer, therefore, only brine water exists in the pore spaces. The water and gas relative permeability was assumed to be functions of their saturations and oil permeability are calculated by using the two-phase relative permeability, water-oil and gas oil, from Equation 2-2 given below:

$$k_{ro} = \left(k_{ro(w)} + k_{ro(wi)} + k_{rw(o)}\right)\left(k_{ro(g)} + k_{ro(wi)} \cdot k_{rg(o)}\right) - \left(k_{ro(wi)} \cdot k_{rw(o)} + k_{rg(o)}\right) \quad (2\text{-}2)$$

Where $k_{ro(wi)}$ is the oil relative permeability measured at irreducible water saturation with no gas present, $k_{ro(w)}$ and $k_{ro(g)}$ is the oil relative permeability calculated at S_o=1-S_w and S_o=1-S_g-S_{wi}, respectively. $k_{rw(o)}$ and $k_{rg(o)}$ are water and gas relative permeability at two-phase water-oil and oil-gas systems (CMG-STARS™).

In this study, there is no oil saturated in the formation, and two phases' relative permeability curves are calculated based on the Brooks-Corey-Burdine Model (Garimella et al., 2019) expressed as following equations (2-3) to (2-5).

$$k_{rw} = s_e^{\frac{2+3\lambda}{\lambda}} \quad (2\text{-}3)$$

$$k_{rg} = \left(1 - s_e^{\frac{2+\lambda}{\lambda}}\right)\left(1 - s_e\right)^2 \quad (2\text{-}4)$$

$$S_e = \frac{(S_w - S_{wr})}{(1 - S_{wr} - S_{gr})} \tag{2-5}$$

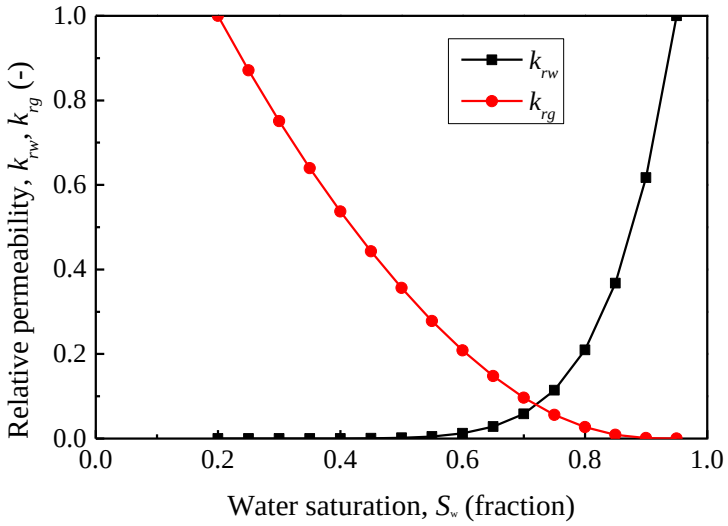

Figure 2-4. Relative permeability curves used in present simulations (Brooks-Corey-Burdine Model) (Garimella et al., 2019)

Where S_e is the effective saturation, k_{rw} and k_{rg} are the aqueous and gas phase relative permeability, S_l is aqueous phase saturation, S_{lr} and S_{gr} are aqueous and gas phase residual saturations, and λ is the pore size distribution index. In present simulations, S_{wr}=0.2, S_{gr}=0.05, and λ=0.5. The relative permeability curve is shown in Figure 2-4. Based on the relative permeability curves, the remaining water saturation after displacement CO_2 gas is almost $S_w \approx 0.65$ which means CO_2 gas saturation becomes $S_g \approx 0.35$ in an aquifer except near the well.

2.3 Definition of pressure and time

The initial pressure of the saline aquifer was set as p_0=10 MPa in this simulation. The BHP in the injection well is equal to p_0+p_i. To analyze the pressure response and distribution of CO_2 saturation in the aquifer for a constant CO_2 mass injection rate q_m (t-CO_2/day) is defined in Figure 2-5.

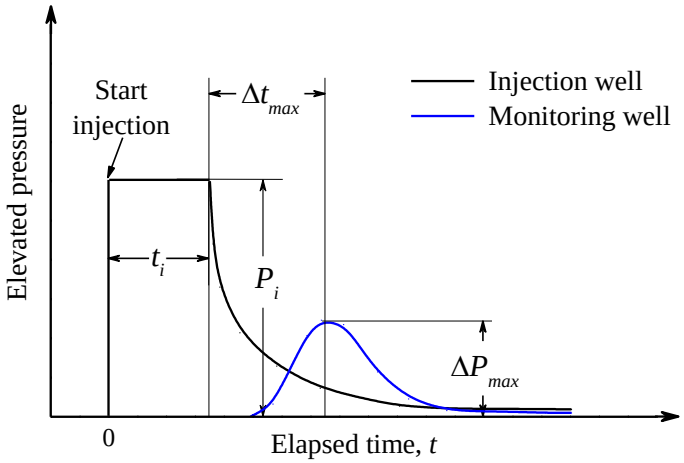

Figure 2-5. Schematic diagram of defined variables

When the injection well is shut-in after the CO_2 injection for a period, t_i, the pressure response of observation well observes the pressure change from the initial pressure with a peak value, Δp_{max} recorded after the delay time, Δt_{max} from the shut-in time at the injection well. The transmission delay time is referred to as the hydraulic diffusivity of the aquifer. The ratio of pressure response at the observation well against the pressure build-up is defined as Equation 2-6 in this study because it shows a pressure transient property reflected by the aquifer reservoir characteristics does not relate to the magnitude of pressure build-up.

$$R = \frac{\Delta p_{\max}}{p_i} \tag{2-6}$$

Simulations were carried out to investigate the pressure response and the delay time of the peak pressure in the observation well with comparing CO_2 plume front position extending to the outer ward.

2.4 Linearized Radial flow equation and estimation solution

Assuming porous media is viscous-dominated and there is no turbulent flow, the flow in porous media can be described by Darcy's law for a single incompressible fluid phase that is shown in Equation 2-7 (Hubbert, 1953):

$$\boldsymbol{q} = -\frac{k}{\mu}\left(\nabla p - \rho g \nabla z\right) \tag{2-7}$$

Where $\boldsymbol{q}$ is the vector of the volumetric flow rate, k (m^2) is permeability, μ and ρ (Pa·s) are the viscosity and density of the reservoir fluid, g is the gravitational acceleration vector directed downwards, ∇p is the hydraulic gradient.

Without considering gravity in the vicinity of an injection well, the governing equation on pressure p (Pa) for one-dimensional radial linearized flow assuming constant compressibility in the aquifer is given as (IEACHG, 2010; Matthews and Russell, 1967; Terry et al., 2015):

$$\frac{\partial^2 p}{\partial r^2} + \frac{1}{r}\frac{\partial p}{\partial r} = \frac{1}{\eta}\frac{\partial p}{\partial t} \tag{2-8}$$

$$\eta = \frac{k}{\phi C_t \mu} \tag{2-9}$$

where η (m^2/s) is hydraulic diffusivity, ϕ is reservoir porosity, μ (Pa·s) is the viscosity of the reservoir fluid, $C_t=C_r+C_f$ (Pa^{-1}) is the total value of rock compressibility (C_r) and reservoir fluid compressibility (C_f), t (s) is the time from the start of CO_2 injection. The hydraulic diffusivity η is a parameter to control unsteady pressure transient.

The pressure build-up in an injection well defined as p_i under the general steady-state radial flow is proportional to the fluid injection rate q (m^3/s) and reservoir fluid viscosity μ, while it is inversely proportional to the transmissivity of the reservoir (Paul et al., 2014) $K=k_r \cdot H$ (m^3) consists of horizontal permeability k_r and the reservoir thickness H. The transmissivity K expresses the ability of fluid flow in the reservoir. The radial flow solution for steady-state ($\partial p/\partial t=0$) in Equation 2-10 is given as the following equation (IEACHG, 2010; Van Everdingen and Hurst, 1949):

$$p_i = p_{wf} - p_0 = \frac{\mu q}{2\pi k H} \ln\left(\frac{r_e}{r_w}\right) \tag{2-10}$$

where p_{wf} is the bottom hole pressure of injection well, p_0 is the initial pressure of the

reservoir, r_e (m) is effective reservoir radius, the extend from injection well to reservoir boundary where the pressure is kept as the initial hydrostatic pressure, r_w (m) is the radius of injection well.

Assuming the reservoir fluid is uniform and uncompressible (C_f=0 and ρ=const), a typical solution of radial transient flow can be written as[31]:

$$p(r,t)\text{-}p_0 = \frac{\mu q}{4\pi kH}\left(\ln\frac{kt}{\phi\mu C_t r^2} + 0.809\right) \tag{2-11}$$

where p_0 is the initial or outer boundary pressure of the aquifer, $q\mu/4\pi kH$ is treated as constant for a constant injection rate q set in the simulations. This solution shows the reservoir pressure build-up in different injection times and different radial distances from the injection. The transient pressure changes in the aquifer at an elapsed time from the start of injection expressed by the transient flow equation can be shown in Figure 2-6.

Assume the pressure response at the observation well at r=r_m is Δp (Pa), it can be estimated by:

$$\Delta p(t) = p(r_m,t)\text{-}p_0 \tag{2-12}$$

The pressure response at an observation well is roughly estimated from pressure changes between build-up and fall-off that are calculated from Equation 2-11 by replacing r=r_m. The transient condition is applicable only if it is assumed that the pressure response in the aquifer is not affected by the presence of the outer boundary, thus the reservoir appears infinite in extent (Dake, 1983). In this study, a constant pressure boundary was assumed that is similar to an infinite reservoir. It is possible to use this equation to estimate rough pressure response at the observation well.

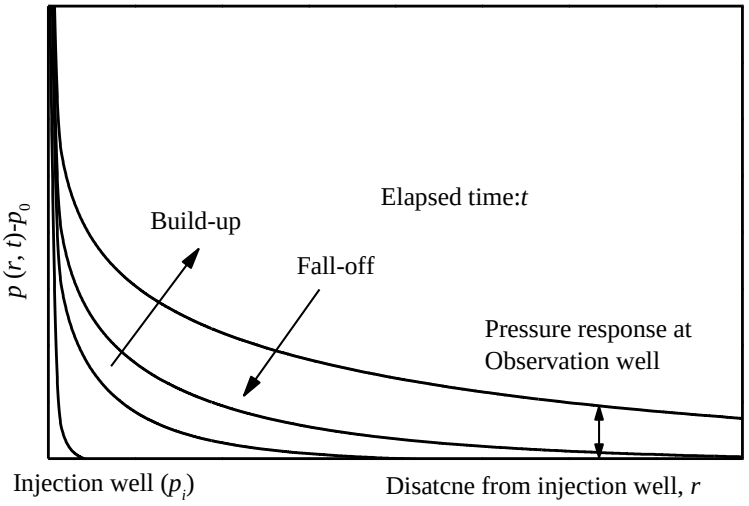

Figure 2-6. Schematic solution showing transient pressure for pressure build-up at an injection well

The distance from the CO_2 injection well ($r=r_m$) is the key parameter to control the magnitude of pressure response at the observation well that is equal to the pressure change in the reservoir due to CO_2 injection from the injection well to analyze the aquifer condition. According to Equation 2-11, the magnitude of the response pressure is proportional to the injection rate q and the injection period t, And the distance from the injection well, defined as r_m, which is almost inversely proportional to the pressure response.

2.5 Injection schemes and parameters setting

2.5.1 Injection schemes

Only one vertical injection well located at the center of the aquifer was defined. The location of the grid blocks containing the injection well. Injected fluid is pure CO_2; therefore, the mole fraction of the injected gas is entered as 1. CO_2 injection temperature is chosen to be equal to the aquifer temperature and injection pressure is chosen as 10-14 MPa so that the injected CO_2 is in the supercritical state.

Two operating constraints are chosen for each simulation. The first operating constraint is the maximum gas injection rate controlled by BHP which must be less

than the threshold capillary pressure and enough below than fracture pressure of the caprock (Fitts and Peters, 2013; Shukla et al., 2010) or upper sealing layer. In the base model, the CO_2 injection rate was kept as q_m=600 t-CO_2/day (q=323448 m^3 std/day, ρ_{CO2}=1.855 kg/m^3 at the surface condition). The second one is the maximum bottom hole pressure to avoid the cap rock fracturing. The maximum BHP has been set as 90% of the threshold capillary pressure (12.6 MPa=14.0 MPa×0.9) measured for the Moebetsu Formation (Hubbert and Willis, 1972).

There are two injection schemes. The single-injection period in the base model was assumed as t_i=100 days, and distributions of pressure response and CO_2 saturation were simulated until t=1,000 days from the start of CO_2 injection. The single-injection scheme is shown in Figure 2-8 (*a*). Another injection scheme is a multiple-injection scheme. As Tomakomai CCS project, the CO_2 injection pattern in the early stage of the project showed the series of injections with multiple pressure build-ups and fall-offs, because CO_2 injection status was tested to check the pressure build-up against the injection rate in the early stage of CO_2 injection. Another injection scheme case to investigate pressure response by the multiple CO_2 injections was shown in Figure 2-8 (*b*). The model includes six injection cycles with t_i=100 days injection and 30 days shut-in based on the Tomakomai CCS project (Singh, 2018).

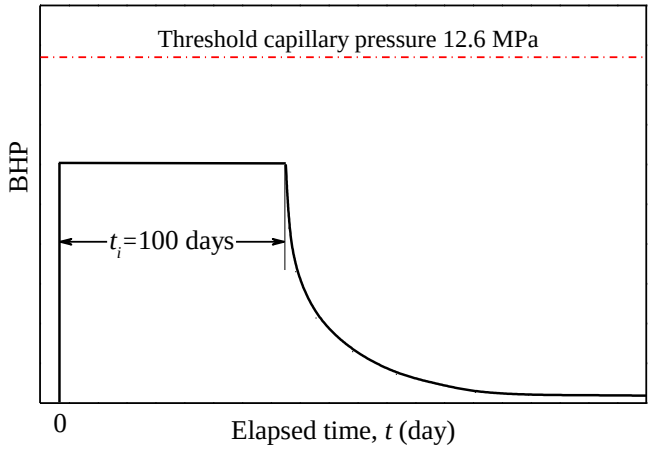

Figure 2-7. The pressure threshold setting for the base model

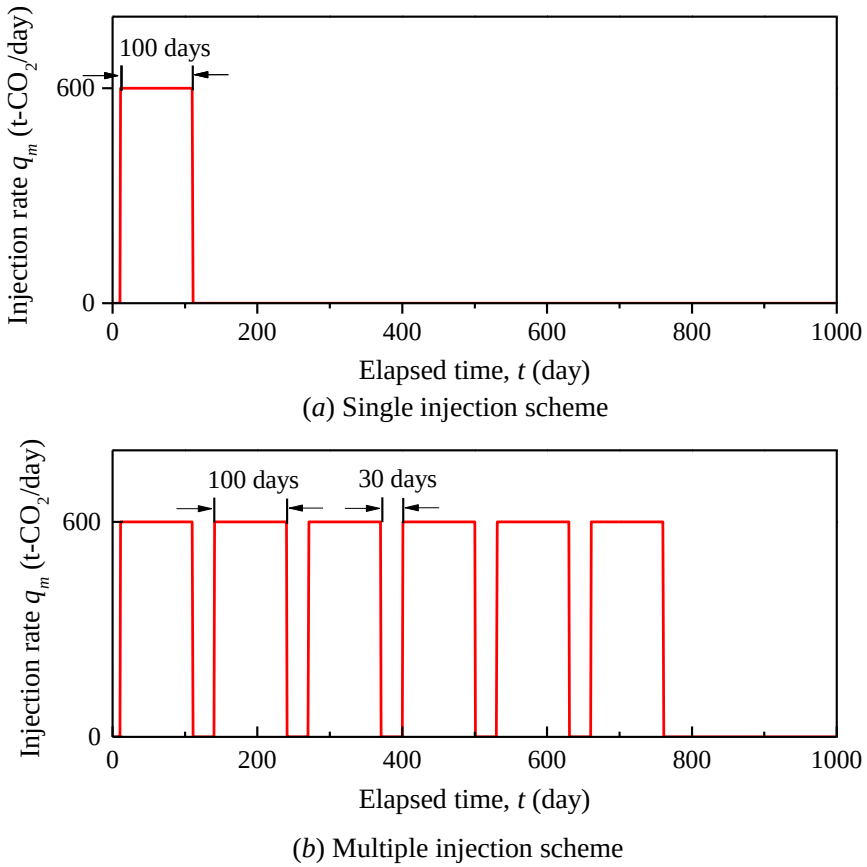

Figure 2-8. Injection scheme for the single injection (*a*) and multiple injections (*b*)

2.5.2 Parameters setting for the simulation study

The simulation parameters set for the base model based on the Tomakomai CCS project are shown in Table 2-2. In the case of Moebetsu Formation targeted in the Tomakomai CCS project, the range of horizontal permeability was estimated as k=0.98 to 980×10^{-15} m^2 (1 to 1,000 md) from the geophysics measurements, and k=3.7×10^{-13} m^2 (=370 md) based on the fall-off test using the injection well after drilling. Also, the porosity was measured as ϕ=0.20 to 0.40 by the laboratory core test and the excavation result is ϕ=0.12 to 0.42 (Tanaka et al., 2014). In this simulation, uniform permeability in the horizontal direction was also set as k_r=370 md, in the horizontal direction, and the ratio of vertical permeability (k_y) to horizontal permeability (k_r) is k_y/k_r=0.1. The porosity ϕ=0.30 was used for the base simulations. No geochemical reactions and mineralization were considered in the simulations due to the short period of fewer than 200 days.

Table 2-2. Aquifer parameters and CO_2 injection well set in the base model (Costa, 2006; Sawada et al., 2018; Szulczewski, 2013; Tanaka et al., 2017)

Parameter	Present Simulation	Tomakomai CCS (Sawada et al., 2018)	Unit (SI)
Aquifer upper level	-1000	-1000~-1200	m
Aquifer thickness, H	100	100~200	m
Outer boundary radius, r_e	10^4		m
Initial aquifer pressure, p_0	10	9.3	MPa
Initial water saturation	1		-
CO_2 injection temperature	40	31.1-40	℃
CO_2 injection pressure, p_0+p_i	<14	4.0-9.3	MPa
CO_2 injection well radius, r_w	0.1		m
Porosity, ϕ	0.3	0.2~0.4	-
Horizontal permeability, k_r	3.7×10^{-13}	3.7×10^{-13}	m^2
Vertical permeability, k_v	3.7×10^{-14}	3.7×10^{-14}	m^2
Rock compressibility, C_r	9.0×10^{-10}		1/Pa
Brine water compressibility, C_w	1.0×10^{-10}		1/Pa
$_{SC}CO_2$ compressibility, C_c	4.0×10^{-10}		1/Pa
Hydraulic diffusivity, η	2.26		m^2/s
Threshold pressure	12.6	12.6	MPa

Note: $_{SC}CO_2$ means CO_2 in the supercritical phase.

2.5.3 Perforation schemes for injecting CO_2

The CO_2 injection well was defined as a vertical well. As different perforation schemes will make a difference in pressure build-up at the well, effects of the perforation scheme on the CO_2 injectivity were discussed. As shown in Figure 2-9, some previous studies used different simulation models with the number of perforation points and their locations for the CO_2 injection (Chadwick et al., 2009; Cinar et al., 2008). In this study, the multiple perforation scheme used 10 holes

perforated in the center of each layer (Fig. 2-9 (*a*)). (Chadwick et al., 2009) used the scheme with the injection point located 10 m below the aquifer ceiling (Fig. 2-9 (*b*)) and carried out the sensitive study on the pressure build-up at the well and pressure distribution in the aquifer. (Cinar et al., 2008) used the scheme with the injection point located in the middle of the reservoir (Fig. 2-9 (*c*)).

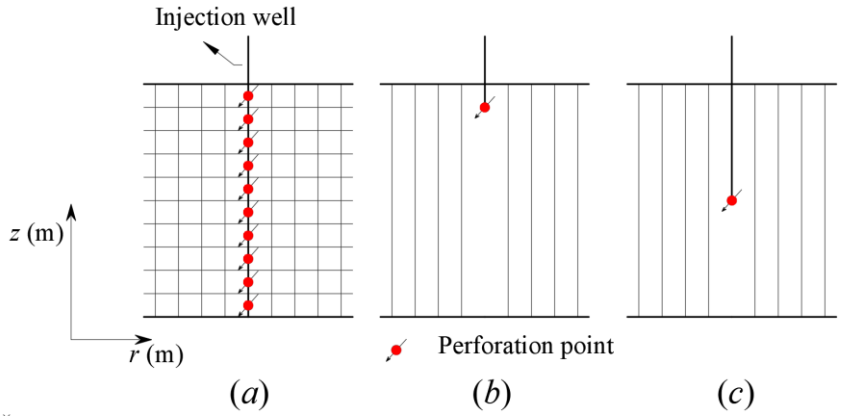

Figure 2-9. Injection well perforation schemes used in previous studies; (*a*) multiple perforations, (*b*) single perforation hole at the top used by (Chadwick et al., 2009), (*c*) single perforation hole at a position used by (Cinar et al., 2008).

Figure 2-10 shows the pressure build-up at the injection well with different perforation schemes for CO_2 injection using the same injection rate. It can be seen that the injection with one perforation point will make a dramatic pressure build-up within the first hour after the start of injection that is more than twice bigger than that of the all perforated injection well (Fig. 2-9 (*a*)). In the multiple perforation scheme, a larger contact area with the reservoir makes smaller pressure build-up and less stress on a sealing layer for the same injection rate. Furthermore, only one block in the vertical direction may not be rigorous to study the pressure build-up. Without considering the pressure gradient of the reservoir, the calculated bottom hole pressure may be overestimated. Therefore, in this study, the multiple perforation scheme was used for all the simulations to make sure a safe injection with smaller pressure build-up at the injection well.

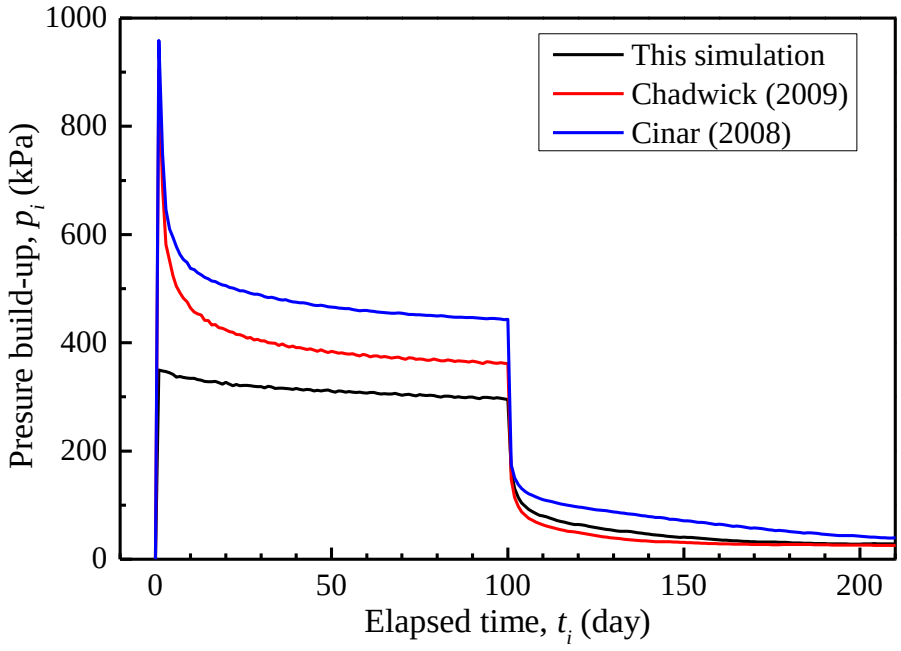

Figure 2-10. Numerical simulation results on pressure build-up at the injection well in different perforation methods of the CO_2 injection well using CMG-STARS™

2.6 Summary

1. In this chapter, a three-dimensional cylindrical describes aquifer model was build-up. The model was referred to as the Moebetsu Formation mainly targeted by the Tomakomai CCS project. The block model consists of (1000, 1, 10) grid cells in the coordinate (radius, azimuth, altitude). As for the Tomakomai CCS project, CO_2 is injected from perforated halls in all wellbore blocks contacting with the aquifer. Specifically, pressure build-up, that is the increase from the initial aquifer pressure (=10 MPa), was controlled less than 2.6 MPa.
2. In the Tomakomai CCS project, 6 sets of CO_2 injection with pressure build-up and pressure fall-off were conducted for 6 months just after the beginning of CO_2 storage, so the injection period (100 to 500 days) and two injection schemes with single and multiple pressure build-up and fall-off were created to compare the pressure response.

3. The approximate prediction method, that uses the analytical solution of the linearized one-dimensional unsteady reservoir flow equation obtained by assuming open boundary, uniform permeability, and uniform fluid saturation, was presented to predict rough pressure build-up, pressure fall-off, and pressure response at a radial position from the injection well. It was shown that the main parameters in the solution are permeability-thickness product, $k \cdot H$, and hydraulic diffusivity, η.

Chapter 3: Numerical simulation results of pressure build-up and fall-off at the injection well and distribution of CO_2 saturation in the aquifer

Pressure build-up and fall-off tests of an oil production well are widely used in petroleum engineering. By the initial injection or production test for a short period, or giving the well some perturbation in the flow rate, the pressure response is measured and matched with the mathematical models. And the matched model can help us to estimate the selected variables combined with the monitoring data.

In the CO_2 geological storage, the well test was also performed. For the saline aquifers, the well test will inject the formation water back to the formation after drilling a well and test the pressure response in the well bottom to analyze the hydraulic properties of the aquifer. For the CO_2 storage case, the injection test by injecting CO_2 is another issue which different from injection saline water into the saline aquifer, it is a two-phase flow issue. In this chapter, the pressure build-up and fall-off of injection well for the single period injection scheme are analyzed by injection CO_2 into the saline aquifer, combined with the numerical simulation some variables were estimated.

3.1 Numerical simulation results of CO_2 saturation in the aquifer

Figure 3-1 shows the simulation results of cross-sectional on r, z axis of CO_2 saturation and CO_2 plume flux vectors at t=10, 50, 100, and 200 days after starting (stopping) CO_2 injection. The CO_2 plume expands mainly as a radial flow, because the horizontal permeability, k or hydraulic diffusivity, η was assumed to be 10 times larger than that of vertical. The buoyancy force on unit CO_2 volume (roughly 4,000 $kN/CO_2\text{-}m^3$) inducing vertical CO_2 convection flow, because of the density difference between injected supercritical CO_2 (around 600 kg/m^3) and saline water (about 1030

kg/m^3) in the aquifer. So, the top layer of the aquifer shows the largest expanding CO_2 seepage flow velocity with the farthest CO_2 plume front. The flow velocity vectors are shown by the red arrow in Figure 3-1. It is clear that the CO_2 plume diffuses mainly in the radial direction during the CO_2 injection period, while the convection in the vertical direction is much slower. After the injection well was shut-in, the driving pressure in the horizontal direction is gradually lost with fall-off pressure, then vertical buoyancy flow becomes noticeable.

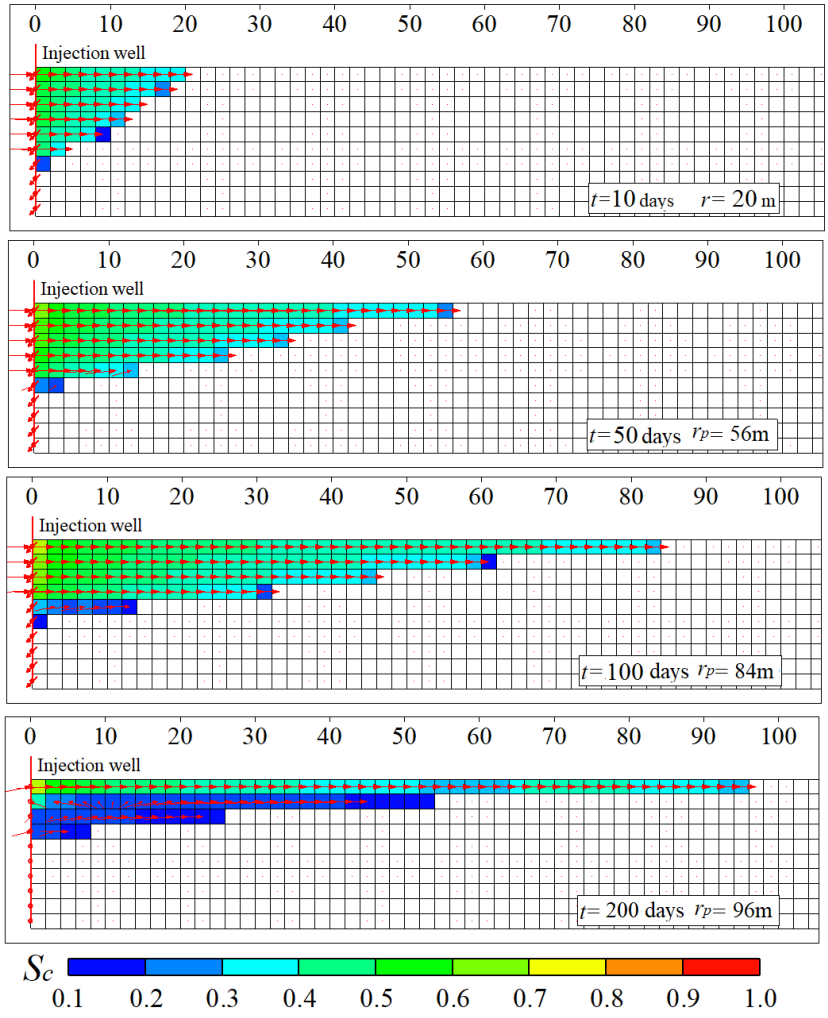

Figure 3-1. Cross-sectional on r, z axis of CO_2 saturation and CO_2 plume flux vectors at t=10, 50, 100, and 200 days for the base model

At the end of CO_2 injection, the CO_2 saturation around the injection well is about 70 to 80 %, and it decreases with the distance from the injection well, especially sharp decrease to 0% around the plume front. After the injection is stopped, the CO_2 pattern

keeps expanding and the CO_2 saturation next to the injection well is decreasing over time. In the case of t_i=100 days, the CO_2 saturation around the injection well decreases to about 50 to 60 % at t=200 days.

We defined the CO_2 plume front at the top layer r_p at where the CO_2 saturation is Sc=0.01. As shown in Figure 3-1, the plume front is observed as r_p=84 m on the 100th day. Figure 3-2 shows the CO_2 plume front position, r_p before and after stopping CO_2 injection at $t=t_i$=100 days. The CO_2 plume front r_p expands almost proportionally to $t^{0.5}$ for $0<t<100$ days, while after the injection well was shut-in for $t>100$ days, the CO_2 front is slowly expanding with proportionally to $0.1t$ by buoyancy force on the CO_2 plume.

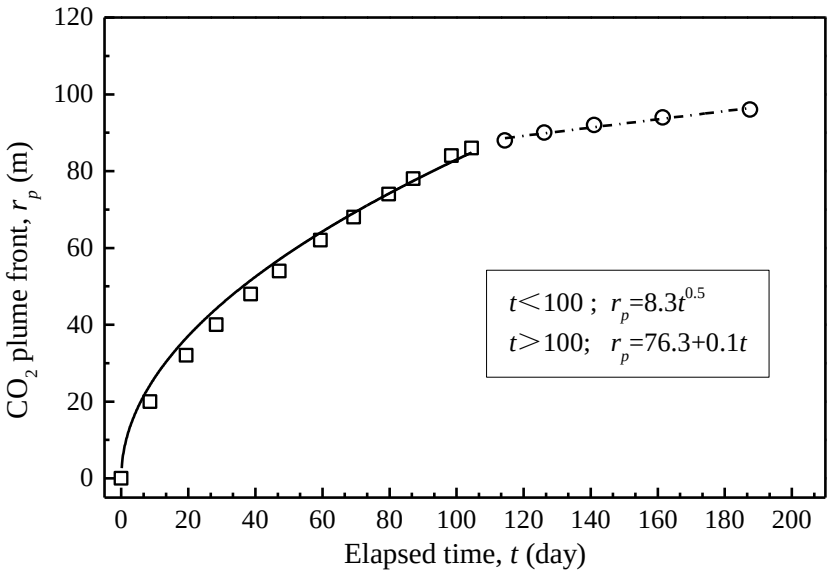

Figure 3-2. CO_2 saturation front distribution over time

3.2 Pressure build-up by injection CO_2

3.2.1 Pressure build-up at the injection well

To study the pressure build-up at CO_2 injection well, an injection scheme based on the base model (q=600 t-CO_2/day and t_i=100 day) with 100 days continuous injection was simulated with comparing the case of injecting saline water that is the initial reservoir fluid. The simulation results are shown in Figure 3-3.

In Figure 3-3, the simulation results were compared with the steady-state flow equation (Eq. 2-9) and transient flow equation (Eq. 2-10). Injecting saline water into the aquifer can be explained as the single-phase flow that the induced pressure build-up is almost the same as the transient flow (r=0.1 m). The injection-induced pressure increases approximately logarithmically with injection time, the maximum pressure build-up is at the end of injection and finally, the reservoir flow turns to be the steady-state flow.

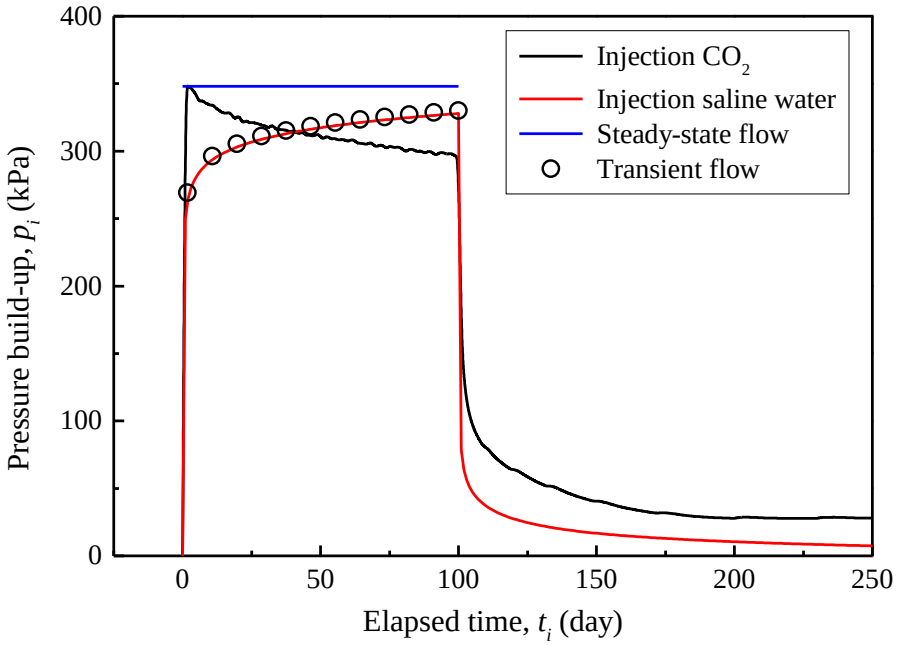

Figure 3-3. Pressure build-up by injecting CO_2 and saline water vs. times for base model

Different from injecting saline water into the aquifer, injecting CO_2 is a two-phase flow issue. By injecting CO_2 into the saline aquifer from an injection well, CO_2 saturation around the injection well is increased with replacing saline water. Therefore, viscosity μ of the aquifer fluid especially around the well is shifting from saline-water viscosity ($\mu_{brine}\approx 6\times10^{-7}$ kPa·s) to supercritical-CO_2 viscosity ($\mu_{CO2}\approx 0.429\times10^{-7}$ kPa·s) gradually with increasing CO_2 saturation. The pressure transient effect was observed during CO_2 injection, especially around the injection well in the early stage of CO_2 geological storage. The BHP during CO_2 injection rises instantly to 350 kPa within an hour after starting the injection, then the pressure is

dropping slowly with CO_2 injection. Because CO_2 saturation value is limited to less than the maximum CO_2 saturation (≈0.35) based on relative permeability curves shown in Figure 2-4 when CO_2 dissolution into saline water is neglected. Therefore, the pressure is dropping during the CO_2 injection time (100 days) is limited to around 50 kPa, even if the CO_2 viscosity is less than 1/10 of the saline water viscosity. Thus, using the brine viscosity in Eq. 2-10 instead of gas viscosity shows a more realistic pressure build-up in the aquifer at the initial injection period. However, the pressure build-up estimated by the Eq. 2-10 using the saline water viscosity will show a little overestimate than using the CO_2 viscosity. This difference also can be explained from the equation presented by Cinar et al. (Cinar et al., 2008; IEACHG, 2010). They modified the steady-state flow equation by introducing the relative permeability of CO_2. However, introducing CO_2 relative permeability is another complicated issue as CO_2 relative permeability is changing with the CO_2 saturation around the injection well, it is difficult to determine the real-time value of CO_2 saturation and this will also add more uncertain variables. In this study, the brine viscosity will be used to estimate rough pressure build-up using Equation 2-10.

In the present simulations, the radial flow consists of saline water and CO_2 is calculated considering relative permeability curves to each fraction. Therefore, physical property changes in the blocks including multi-phase flow are simulated automatically in the present simulations using CMG-STARS^{TM}.

Numerical simulation results for the base model on the distributions of reservoir pressure change from initial aquifer pressure ($p(r)$-p_0) compared with the CO_2 saturation (Sc(r)) at t=50 and 100 days are shown in Figure 3-4.

It can be seen that pressure changes and CO_2 saturation distributions are correlated in the region of CO_2 saturation Sc>0.35, while only pressure changed by the convection of CO_2 and saline water is observed in the region (r<84 m) with CO_2. Assuming the position of the CO_2 plume front defined by Sc=0.01, the pressure transmitting speed is much higher with two order times than that of the CO_2 plume front, because the

pressure change is observed without CO_2 saturation change.

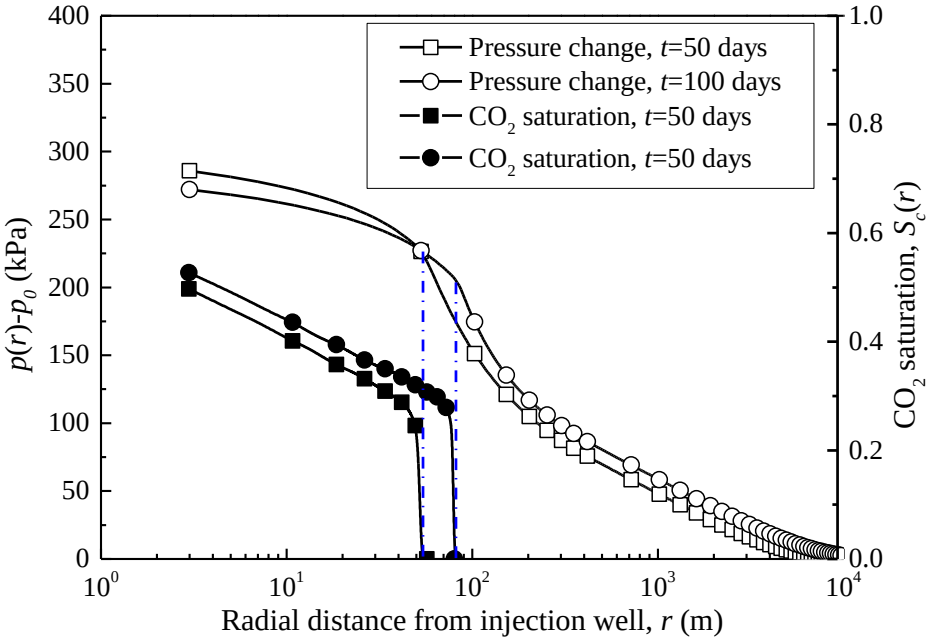

Figure 3-4. Numerical simulation results of pressure response vs. CO_2 saturation at different distances from the injection well

3.2.2 Effect of CO_2 injection rate on pressure build-up

Figure 3-5 shows the simulation results of pressure build-up, p_i at the CO_2 injection well for injection rate, q_m comparing with the estimated line calculated using Equation 2-10 by assuming saline water viscosity discussed in the last section. The pressure build-up does not show a significant linear relationship with injection rate. As discussed in the above section, this can be explained by the changing CO_2 saturation around the injection well, since the relative permeability changed with CO_2 saturation. The simulation results show that the linearity between p_i and q_m is better and closer to estimated values by Equation 2-10 in a low injection rate q_m<600 t-CO_2/day than that in a large injection rate q_m>1,500 t-CO_2/day because the higher injection rate results in a faster change of CO_2 saturation around the injection well.

We have confirmed that the estimated pressure build-up by using saline water viscosity can be corrected by using a viscosity of 65% of saline water one because the CO_2 saturation around the injection well is close to 0.35.

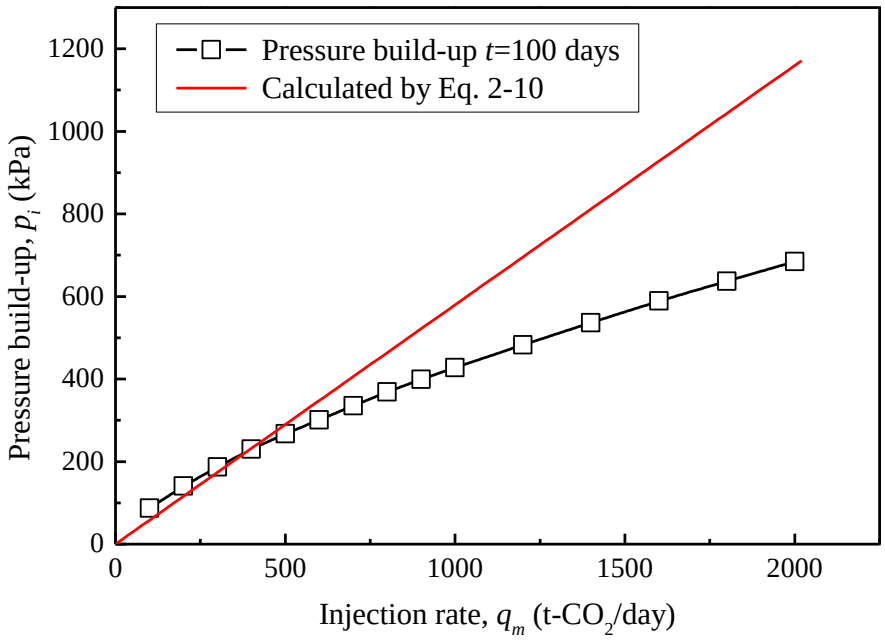

Figure 3-5. Numerical simulation results of pressure build-up pi vs. CO_2 mass injection rate q_m

3.2.3 Estimation of transmissivities of Moebetsu formation

The CO_2 testing injection into Moebetsu Formation was conducted between April 6th and May 24th, 2016 with 180 to 600 t-CO_2/day in injection rate and 7,163 t-CO_2 in cumulative amount. The recorded pressure build-up data are collected on the website and shown in Figure 3-6 (Japan CCS CO., 2016-2020) and the maximum pressure build-up of injection well (IW-2) was recorded around p_i=450 kPa at the injection rate q_m=600 t-CO_2/day and total injection time t_i=50 days. So, the simulation was run with the injection period t_i=50 days, and the parameter setting was based on the base model (injection rate q_m=600 t-CO_2/day). The thickness of Moebetsu formation is around 100 to 200 m which is uncertain and is different from the base model set, simulations were run and the pressure build-up against different transmissivities of aquifers was summarized in Figure 3-7. And the field pressure data were compared with the simulation results to estimate the transmissivity of Moebetsu formation.

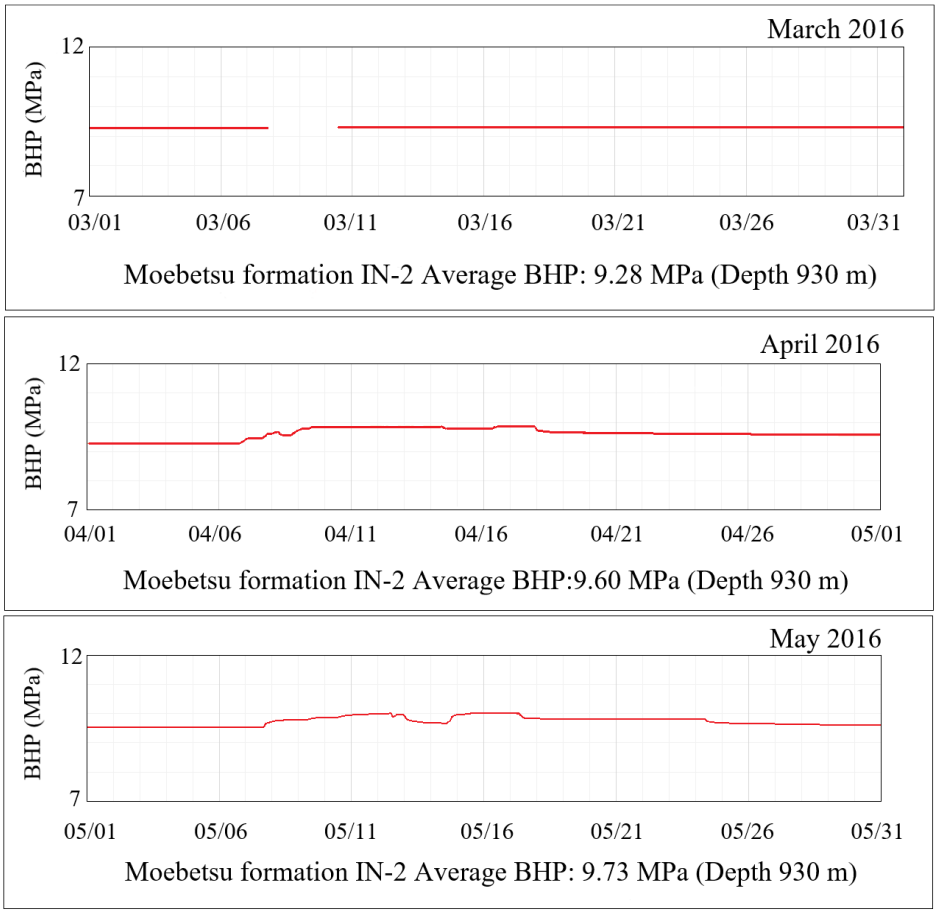

Figure 3-6. The monitoring data of testing CO_2 injection into Moebetsu formation (April 6th and May 24th, 2016)

According to the simulation results shown in Figure 3-7, the transmissivity of Moebetsu formation is about K=2.7×10^{-11} m^3, and the permeability of the Moebetsu formation was calculated as k=1.35×10^{-11} to 2.7×10^{-11} m^2 (135 to 270 md) which is different from our base model setting k=3.7×10^{-11} m^2 (=370 md). The permeability of the aquifer is 370 md is overestimated by comparing the field pressure data and simulation results. Due to the short injection period, the fluid flow around the injection well is in an unsteady state. In Figure 3-7, the pressure build-up at the injection well after 1 day and 50 days vs aquifer transmissibility (K) were compared with those in the steady-state flow (Eq. 2-10). As in the early stage of injection, there is a transient effect of pressure build-up at the injection well, pressure build-up of injection well on the 1st day is larger than on the 50th day and this difference will be larger in a reservoir with high transmissivity. The pressure build-up of the injection

well on the 50th day is closer to the steady-state flow compared with that on the 1st day. An aquifer with higher transmissivity is getting closer to the calculated pressure build-up, p_i of steady-state flow.

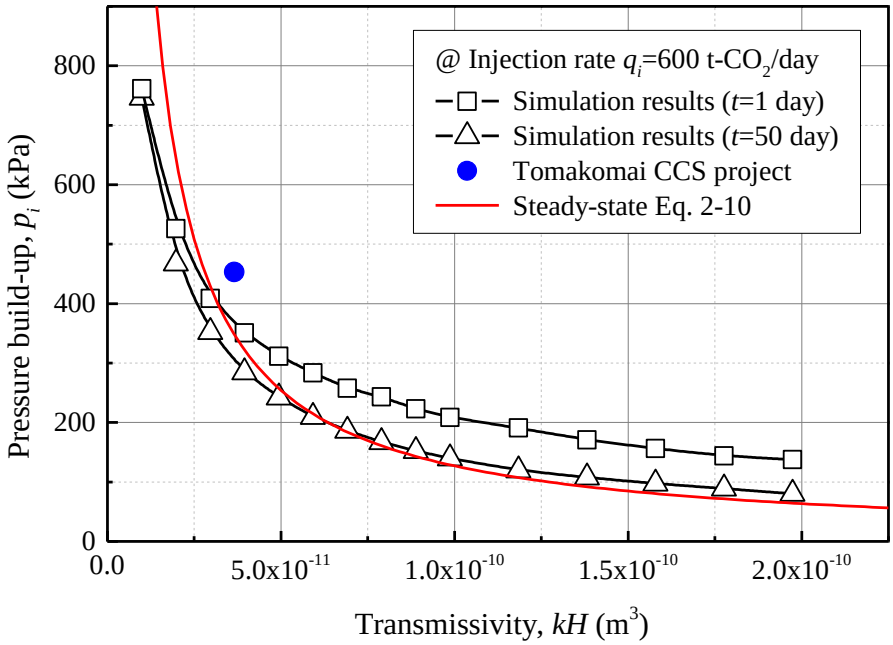

Figure 3-7. Pressure build-up, p_i (kPa) vs. aquifer transmissibility, $k{\cdot}H$ (m^3)

3.3 Pressure fall-off at the CO_2 injection well after shut-in

Opening or shut-in a well causes pressure changes in the CO_2 injection well. In the CCS projects including fall-off data after shut-in has a possibility to study the aquifer state. When bottom hole pressure fall-off lines of BHP vs. time (Kazemi et al., 1972) are measured with enough precision after the well shut-in, the aquifer *in-situ* permeability and well skin factor can be estimated by analyzing the data. It is similar to the well testing method widely used in petroleum reservoir engineering. Without considering the skin factor the pressure fall-off function in the injection well is expressed by the radial transient flow equation (Eq. 2-11). For the pressure fall-off testing, the pressure p_0 in Eq. 2-11 should be modified to the instantaneous bottom hole pressure when the injection well was shut-in. Because $q\mu/4\pi Hk$ can be treated as a constant for a constant injection rate q, the hydraulic diffusivity η can be focused as the main parameter that controls the fall-off curve.

Different from the traditional method of analyzing pressure fall-off lines, the pressure fall-off time is defined in this study to analyze reservoir conditions and pressure transient. As shown in Fig. 3-8, $t_{0.75}$ and $t_{0.25}$ are defined the elapsed times to reach 75% and 25% pressure reductions from the build-up pressure when the well was just shut-in. Then pressure fall-off time is defined as $t_{0.75}$-$t_{0.25}$ that shows the period the build-up pressure p_i falls 50%.

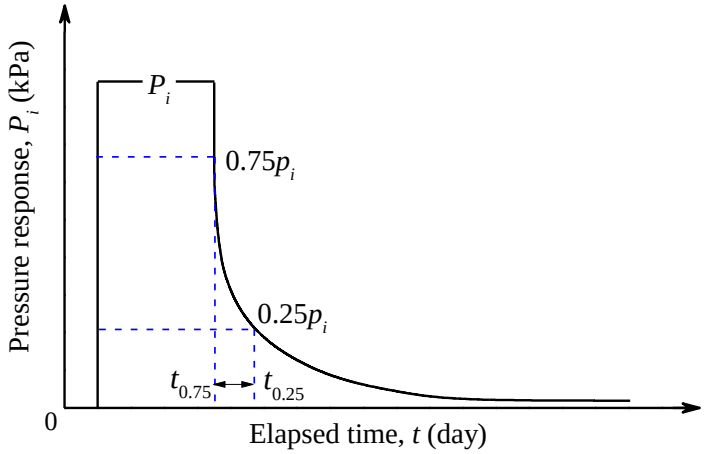

Figure 3-8. Definition of pressure fall-off time from pressure build-up

In the case of CO_2 injection in Moebetsu formation, Tomakomai CCS project, some pressure fall-off data were recorded after shut-in the well, and the fall-off time ($t_{0.75}$-$t_{0.25}$) were analyzed as about 5 days based on the BHP data(Dietz, 1965; Escobar and Montealegre-M, 2008). The numerical simulation results on the fall-off time ($t_{0.75}$-$t_{0.25}$) vs. hydraulic diffusivity η for the base model are shown in Fig. 3-9 that includes the results of different porosity (0.1, 0.2, and 0.3) and permeability k=1×10^{-13} to 20×10^{-13} m^2 (100 md-2,000 md). As the fall-off time was about 5 days for the Moebetsu formation (dotted line in Fig. 3-9), the hydraulic diffusivity range of Moebetsu formation can be estimated as η=2 to 4 m^2/s from the simulation results between ($t_{0.75}$-$t_{0.25}$) and η. As the transmissivity of Moebetsu formation was matched as K=kH=2.7×10^{-11} m^3 in the last section, and the thickness is between H=100 to 200 m, porosity ϕ=0.2 to 0.4, therefore the matrix rock compressibility of the Moebetsu formation is estimated as C_r=0.14×10^{-9} to 1.11×10^{-9} Pa^{-1}. This means that the rock compressibility set as C_r=0.9×10^{-9} Pa^{-1} is within the reasonable range compared with

the Moebetsu formation.

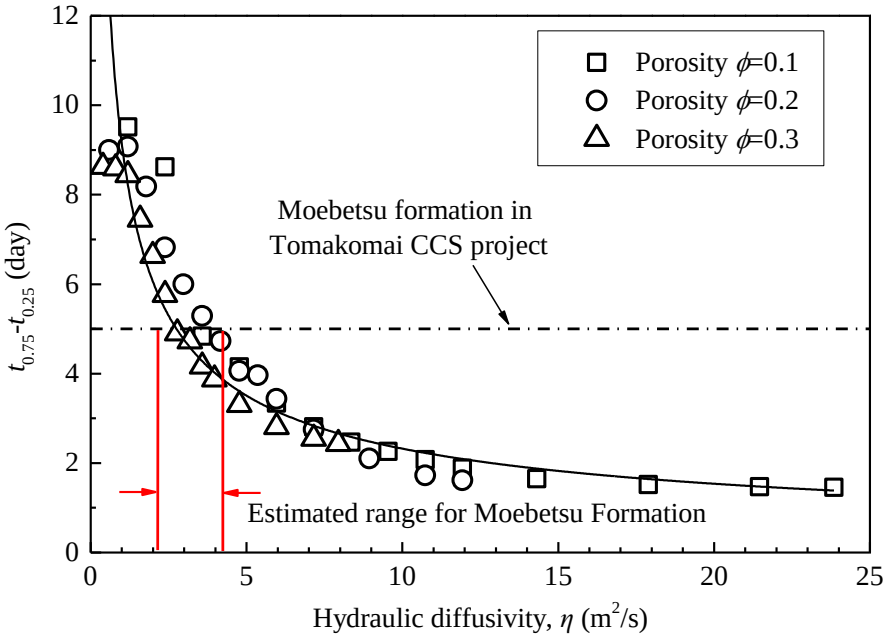

Figure 3-9. Numerical simulation results on fall-off time ($t_{0.75}$-$t_{0.25}$) vs. hydraulic diffusivity η compared with the fall-off time of Moebetsu formation (5 days)

3.4 Summary

In this chapter, the pressure build-up and fall-off of a single injection scheme were studied after performing CO_2 injection for a certain period (50 to 500 days). The numerical simulation results for pressure build-up and fall-off in the injection well conclusions are summarized below:

1 The CO_2 plume expansion radius of the top is r_p=84 m at t=100 day. The CO_2 plume front r_p expands almost proportionally to $t^{1/2}$ before $t<t_i$. After shut-in the injection well ($t>t_i$), the front is slowly expanding proportionally to 0.1t due to the buoyancy force on the CO_2 plume. In addition. The CO_2 saturation around the injection well increases to about 0.35 with the elapsed time and reduces the effective fluid viscosity.

2 The increase in pressure build-up was inversely proportional to $k{\cdot}H$. However, the decrease in pressure build-up is about 5% compared to the case of saline water. It was the reason that the CO_2 saturation in the aquifer is

limited by the irreducible water saturation of 0.65, and pressure build-up does not decrease significantly even if the CO_2 viscosity is less than 1/10 of water.

3 The transmissivity of Moebetsu formation is estimated as 2.7×10^{-11} m^3 and the hydraulic diffusivity of the reservoir is 2-4 m^2/s by the analysis of pressure build-up and fall-off. Assuming the permeability is $k=1.35\times10^{-11}$ to 2.7×10^{-11} m^2 (135 to 270 md) and the porosity is 0.2 to 0.4 of the Moebetsu Formation, the matrix rock compressibility of the Moebetsu formation is estimated as $C_r=0.14\times10^{-9}$ to 1.11×10^{-6} Pa^{-1}. It was confirmed that the time required to reduce by half the pressure build-up decreases exponentially with increasing η.

Chapter 4: Numerical simulation results of pressure response at the observation well for single build-up and fall-off

The pressure response at observation well was studied. Both pressure build-up at the injection well and pressure response at the observation wells have almost linear relationships to the injection rate when the injection rate q_m<600 t-CO_2/day.

The pressure ratio $R=\Delta p_{max}/p_i$ of pressure build-up at the injection well and the pressure response at the observation well was analyzed. It is not sensitive to the mass injection rate, q_m. It is only proportional to injection period (t_i), hydraulic diffusivity (η) and is inversely proportional to the square of radial distance from the well.

4.1 Pressure response at observation wells

CO_2 injection will induce a pressure disturbance in the aquifer, and the pressure spread much faster than the CO_2 plume. In general, an observation well is drilled far away from the CO_2 injection well to monitor the pressure change induced by CO_2 injection at the well bottom. By comparing the recorded pressure build-up at the injection well and the response pressure at the observation well in the well bottom, the safety of storage can be estimated.

As is shown in Figure 4-1, after the injection well is shut-in, the pressure wave will diffuse to the out word and a peak pressure $\Delta p_{\max}$ will be recorded with the distance r from the injection well. In this section, the pressure response at hypothetical observation wells located at a range of radial distance r_m=1,000 m to 5,000 m from the injection well was discussed based on the simulation results. The simulation results were compared with the estimated values using Eq. 2-12 presented in chapter 2. The maximum value of pressure response is defined as Δp_{max} that is recorded at the observation well ($r=r_m$) after 100 days continuous CO_2 injection in each injection scheme. The analytical equation assuming transient radial flow using Eq. 4-1 as

expressed by:

$$\Delta p_{max} = p(r_m, t_i) - p_0 \quad (4\text{-}1)$$

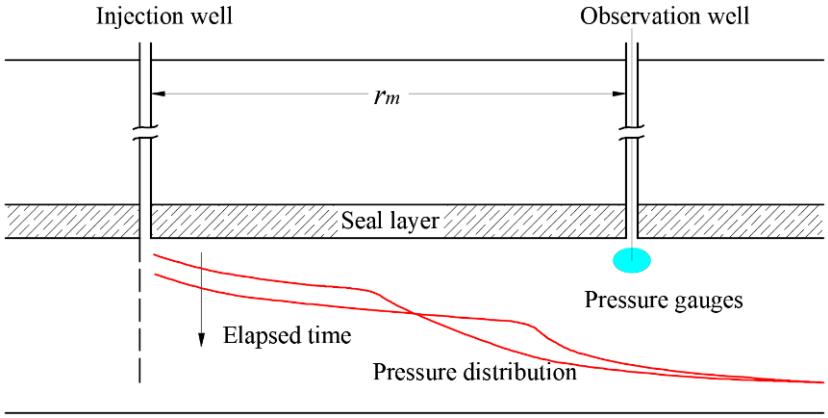

Figure 4-1. The pressure diffusion after the injection well is shut-in

Figure 4-2 shows the numerical simulation results of the pressure response at the observation well r_m=1,000, 3,000, and 5,000 m against the CO_2 mass injection rate q_m=600 t-CO_2/day for t_i=100 days (base model). The response pressure at the observation well location increases gradually during the injection period and fall off with a delay time after the injection well was shut-in. The pressure build-up at observation well is different from that at the injection well. This is because the pressure build-up at the injection well (less than r=100 m) is influenced by both CO_2 and saline water flows, while the pressure response at the observation well far from the injection well is not influenced by the difference of CO_2 and saline water viscosity. After the injection well is shut-in ($t>t_i$), the observation well pressure draws a fall-off curve similar to the pressure fall-off of the injection well. The peak value of the response pressure, Δp_{max} becomes smaller and broader, and the peak time after the injection well was shut in recorded at the observation well, Δt_{max} increases with the increasing distance from the injection well, r_m. For example, Δp_{max}=25 kPa at r_m=3,000 m becomes almost half of Δp_{max}=57 kPa at r_m=1000 m. The observation well at r_m=1,000 m will response the peak pressure value in a day, while it will take about 15 days for the observation well at r_m=1,000 m to reach the peak pressure value.

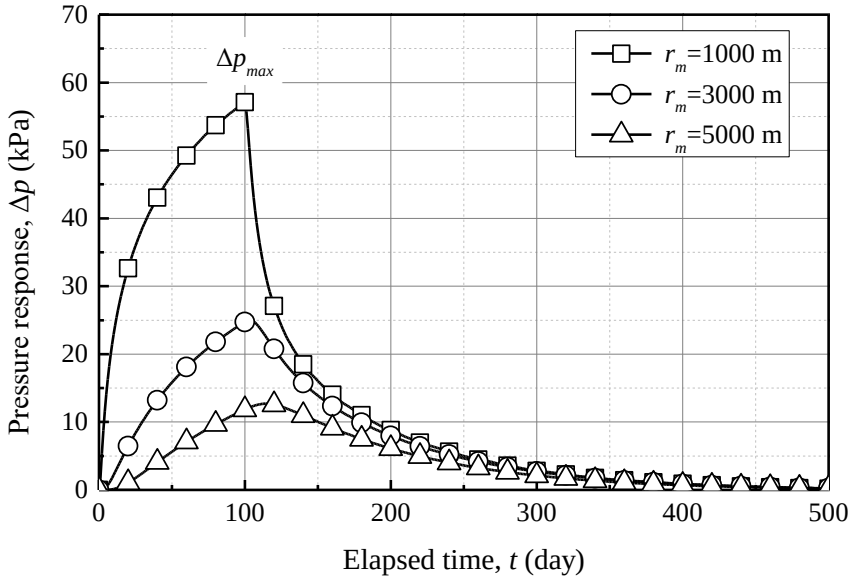

Figure 4-2. Typical simulation results of the pressure response at observation well located at r_m=1,000, 3,000, and 5,000 m

As is shown in Figure 4-3, different from the pressure build-up at the injection well, the simulation results of pressure response Δp_{max} have a good linear relationship with the CO_2 mass injection rate q_m as the same as the numerical simulation results for injecting saline water.

The analytical solution of Eq. 4-1 is smaller than the simulation results. These differences become larger with the increasing radial distance between the injection well and observation wells because the estimated value by the Eq. 4-1 can only be applicable for a rough estimation. In this simulation study, the injection period was assumed as t_i=100 days, and the detectable peak pressure response at the observation well will also need several days after the injection well is shut-in. The time t for analytical solution Eq. 4-1 was assumed the same as the injection period t_i. As has been discussed before, there was a time delay for the observation well response to the peak pressure, and the time delay becomes larger for the observation well with a larger distance from the injection well. So, the differences between the simulation results and Eq. 4-1 will become larger.

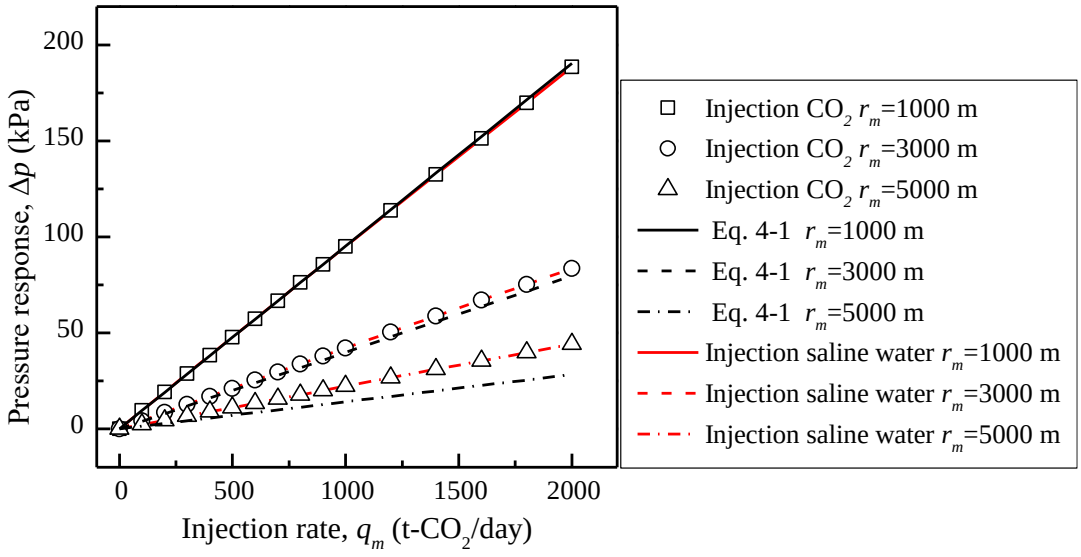

Figure 4-3. Numerical simulation results on pressure response of observation well vs. CO_2 mass injection rate q_m (t-CO_2/day)

4.2 The pressure ratio of the build-up pressure in injection well and the response pressure in the observation well

To avoid the error in the absolute magnitude of the pressure response at the observation well, we introduced a ratio R between pressure build-up at the injection well p_i and the maximum value of pressure response at the observation well Δp_{max} as defined by Eq. 4-1. Both pressure build-up at the injection well and pressure response at the observation wells have almost linear relationships to the injection rate, q_m<600 t-CO_2/day. This ratio is very useful to find pressure response at the observation wells based on the pressure build-up data at the injection well, because the ratio $R=\Delta p_{max}/p_i$ is not sensitive to the injection rate, q_m. Besides, the term of $q\mu_w/4\pi Hk$ in Eq. 2-10 can be treated as constant for a constant mass injection rate q_m. So, the value of R is only proportional to injection period (t_i), hydraulic diffusivity (η) and is inversely proportional to the square of radial distance from well, while it is not so sensitive to the CO_2 mass injection rate q_m. The rough value of R can be estimated by the following equation and hydraulic diffusivity η defined by Eq. 4-2.

$$R=\frac{1}{2\ln(r_e/r_w)}\left(\ln\eta\frac{t_i}{r_m^{\,2}}+0.809\right)$$
$$=0.0434\cdot\left(\ln\eta\frac{t_i}{r_m^{\,2}}+0.809\right) \quad (4\text{-}2)$$

where C_t is equal to rock compressibility because fluid is assumed to be incompressible in the transient flow equation (C_f=0), r_e=10,000 m is the effective reservoir radius and r_w=0.1 m is the radius of injection well. The Eq. 4-2 shows that R consists of a logarithmic function of time t, aquifer area up to the inner area of the observation well radius (πr_m^2), and hydraulic diffusivity, η. Assuming the observation well will respond to the peak pressure value at the moment the injection well is shut-in, and the time t in Eq. 4-2 is replacing with t_i.

The numerical simulations on R using CMG-STARS were done for the base model with the horizontal permeability range from k=2 to 8×10^{-13} m^2 (=200 to 800 md), the observation well location r_m=1,000 to 5,000 m and different injection periods t_i=50 to 300 days, porosity and compressibility of porous media are considered constant (ϕ=0.3 and C_t=1.4×10^{-6} 1/kPa). The sensitive study of hydraulic diffusivity η was also carried out by setting the constant injection rate q_m=600 t-CO_2/day. The simulation results of R are shown in Figure 4-4 with comparing values calculated by Eq. 4-2. It can be seen that the pressure ratio R shows the almost logarithmic function of $\eta t/r_m^2$. However, there is a little difference between the values of R for different permeability, especially in $\eta t/r_m^2$>10. Because there is a time delay from the injection well is shut-in to the observation well response the peak pressure value, the time t of the simulation results shown in Figure 4-4 were considered as $t=t_i+\Delta t_{max}$. And Δt_{max} is defined as a time delay from the shut-in time at the injection well to the observation well reach the peak pressure. Thus, the pressure response at the observation well calculated by Eq. 4-2 shows underestimated compared with the numerical simulation, however, both of R vs. $\eta t/r_m^2$ looks similar relationship expressed by a logarithmic function. And it also can be seen that Eq. 4-2 is more suitable for a high permeability aquifer. As, it takes a shorter time for an aquifer with a larger permeability, and the

simulation results of R will be closer to the value calculated by Eq. 4-2. This logarithmic function can help us to make an evolution of the pressure at the observation well in different distance r_m, at a different time according to the injection well pressure build-up of field data. In the study in chapter 3, the hydraulic diffusivity η was evaluated by the pressure fall-off lines after the shut-in. So, the observation well location can be designed with a proper distance and selecting a pressure transmitter with suitable pressure resolution for the pressure monitoring.

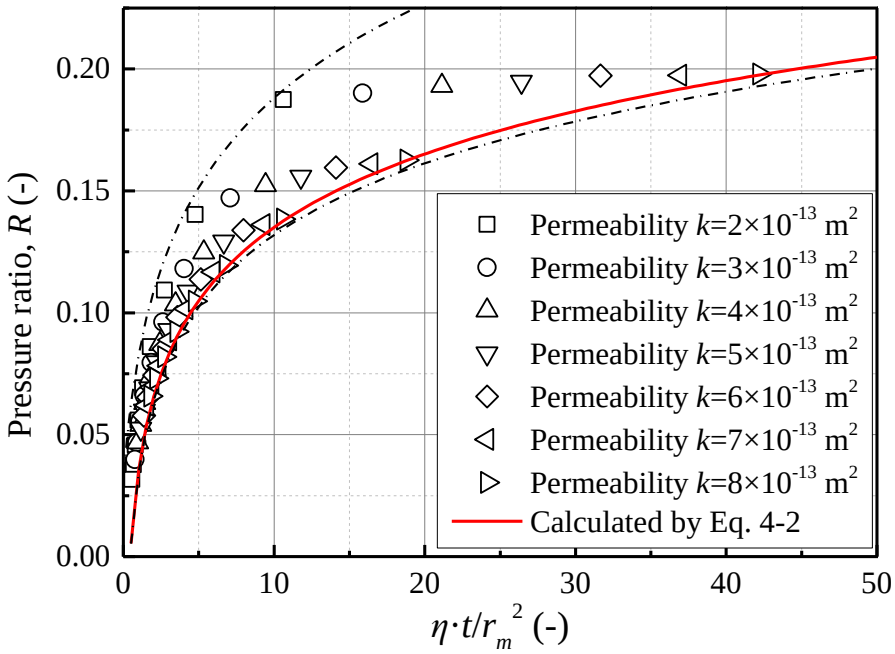

Figure 4-4. Numerical simulation results of pressure ratio R for different permeability (q=600 t-CO_2/day, t_i=100 days, k=2 to 8×10^{-13} m^2 (=200 to 800 md))

An empirical equation base on the simulation results in Figure 4-4 was summarized without considering the time delay Δt_{max}, and it is given by:

$$R=\frac{\Delta p_{\max}}{\Delta p}=(0.0425\text{-}0.06)\cdot\left(\ln\eta\frac{t_i}{r_m^{\,2}}+0.809\right) \tag{4-3}$$

The pressure ratio at an observation will have a big variation at different permeability aquifer conditions. The equation 4-3 is summarised of the simulation results based on the Tomakomai CCS project and simulated with different permeability cases and it can also be used to estimate other CCS projects in the pressure ratio $\eta t/r_m^2$<10 that

has smaller deviation with different permeability reservoir. Besides, specific analysis about the pressure ratios against different variables can be done by simulation studies to make a relatively more accurate assessment for a planned CCS projects in the future.

According to the simulation results of pressure build-up at the CO_2 injection well and pressure response at the observation well, it is expected that the pressure ratio R increases with the increasing injection period because the pressure build-up at the injection well p_i decreases with increasing the CO_2 injection period t_i, while the response pressure at the observation well Δp_{max} becomes higher. Figure 4-5 shows the numerical simulation results of the pressure ratio R for different injection period t_i=50 days to 300 days. The higher response pressure can be monitored by increasing the injection period because R increases with t_i.

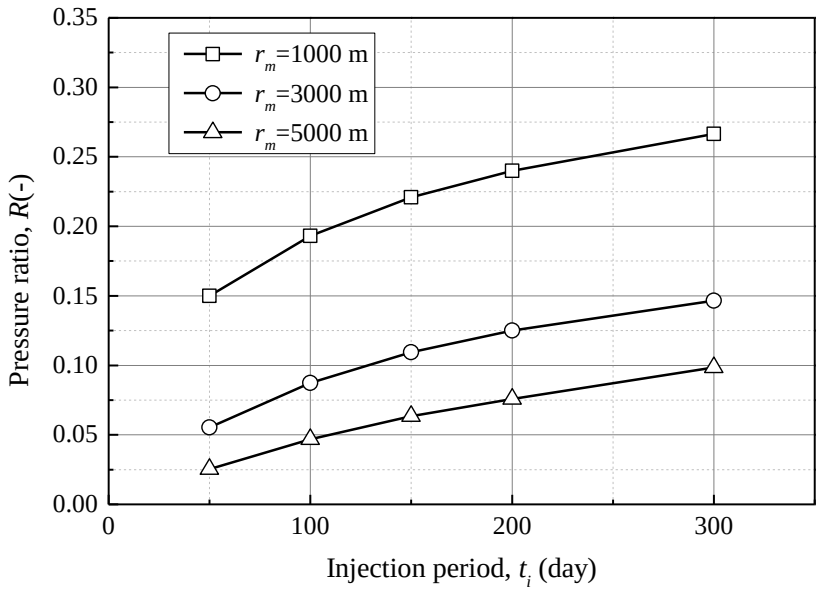

Figure 4-5. Effect of injection period, t_i on pressure ratio, R

The pressure ratios in different distances from the injection well for the base model are shown in Figure 4-6, compared with the pressure ratio in an aquifer with permeability k=10^{-13} m^2 and 8×10^{-13} m^2. The pressure fluctuates with the permeability of the aquifer. As is analyzed according to Figure 4-4, there is a little difference between the values of R for different permeability, especially in $\eta t/r_m^2$>10. Figure 4-

6 is more intuitively reflecting the pressure ratio changing with the radial distance from the injection well. The pressure ratio, R shows a larger difference in permeability when the radial distance from the injection well is larger. However, as the upper limit of pressure response at the observation well is small, it is easy to estimate pressure for choosing an effective pressure sensor. In the case of the Tomakomai CCS project, the observation well OB-2 drilled at r_m≈3,000m from the injection well to monitor the pressure change caused by CO_2 injection. The present simulation result for q_m=600 t-CO_2/day and t_i=100 days shows that R=0.09 at r_m=3,000 m.

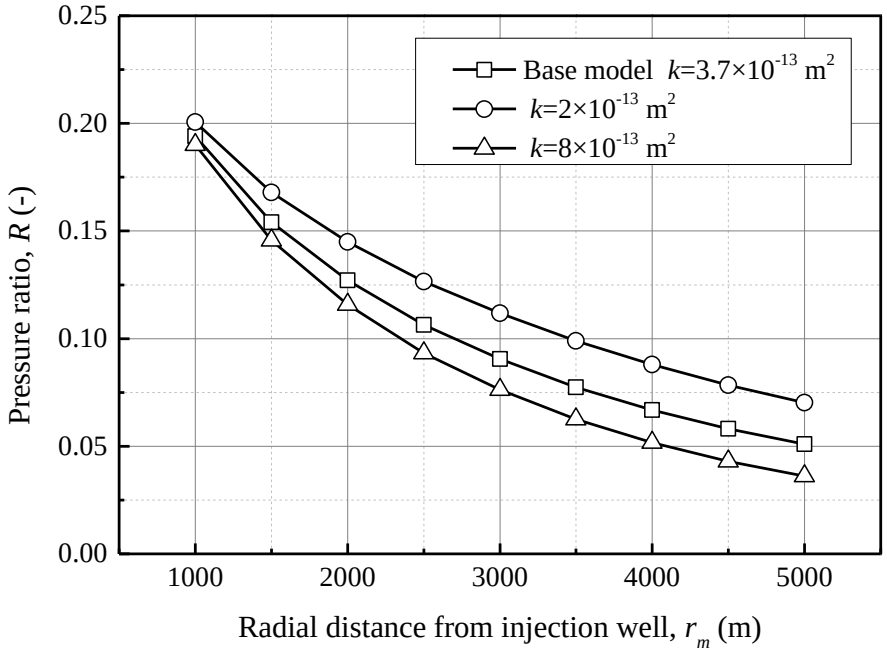

Figure 4-6. Pressure ratio vs radial distance from injection well (t_i=100 days) for the base model

4.3 Delay time of the pressure response at the observation well

Even if the injection well is shut-in and return to the initial pressure, the pressure transmitting in the aquifer continues moving to the outer ward with depleting its amplitude. Figure 4-7 shows the numerical simulation results of time delay Δt_{max} in the aquifer with the horizontal permeability range from k=2 to 8×10^{-13} m^2 (=200 to 800 md) at the observation wells with different radial distances (r_m=1,000 to 5,000 m) from the injection well. As has been discussed above, fluid flow transmits fast in

a high permeability aquifer, the pressure transmitting speed is much higher with two order times than that of the CO_2 plume. The time delay Δt_{max} is proportional to the radial distance from the injection well and inversely proportional to the aquifer permeability. The time delay Δt_{max} increases exponentially with increasing the radial distance r_m. For example, the time delay for the observation well located in the radial distance r_m=1,000 m responses to the peak pressure value in a day of shut-in injection well, while it takes about 37 days for the observation well located in the radial distance r_m=5,000 m to response the peak pressure for a reservoir with permeability k=2×10^{-13} m^2 (=200 md).

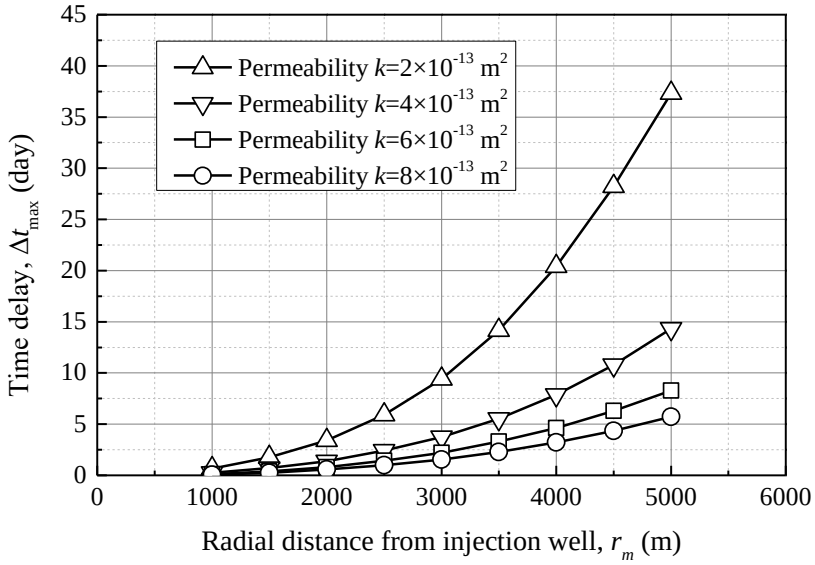

Figure 4-7. Numerical simulation results of time delay Δt_{max} of the pressure response peak to arrive at the observation well located at the radial distance rm (Base model, injection period t_i=100 days)

Figure 4-8 shows the numerical simulation results of time delay Δt_{max} in the aquifer with the injection rate range from q_m=200 to 800 t-CO_2/day at the observation wells with radial distances r_m=3,000 from the injection well. It is the same as the pressure ratio that the delay time is also not sensitive to the injection rate. The time delay Δt_{max} at the observation well r_m=3,000 m is the same in different injection rates.

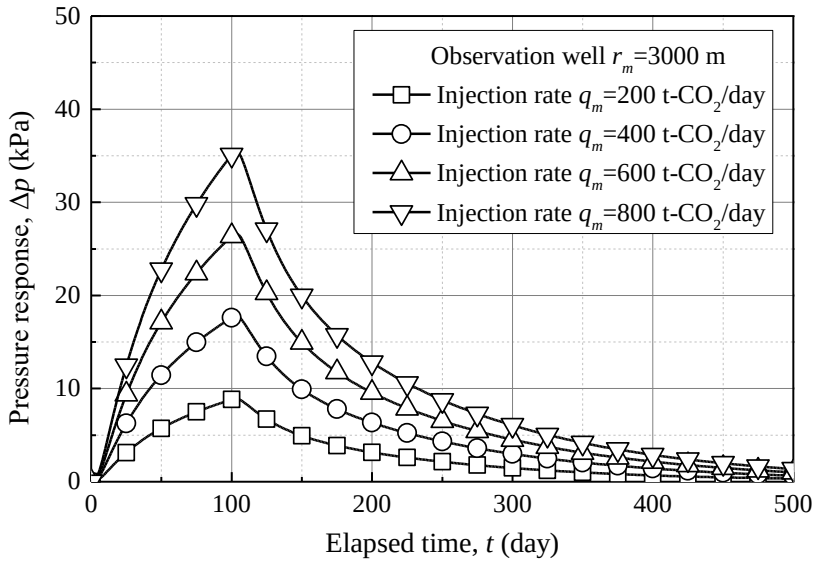

Figure 4-8. Numerical simulation results of time delay $\Delta t_{\max}$ of the pressure response peak to arrive at the observation well r_m=3,000 m vs different injection rate (q_m=200-800 t-CO$_2$/day)

The pressure response at the observation well shows the peak pressure which is almost proportional to the pressure build-up at the injection well. On the other hand, the delay time, Δt_{max} as defined before was found as the peak value on the line of $p(r_m)$ vs. t by setting r_m=1,000 m to 5,000 m and permeability k=2×10^{-13} m^2 to 8×10^{-13} m^2 (=200 to 800 md).

The simulation results of Δt_{max} vs. r_m^2/η were summarized in Figure 4-9. It can be seen that the time delay $\Delta t_{\max}$ shows almost linearly proportional to r_m^2/η that is reverse proportional to horizontal permeability, k. Those relationships can be summarized as the following equation:

$$\Delta t_{\max} = 0.13 \cdot \frac{r_m^2}{\eta} = 0.13 \cdot \frac{\phi C_t r_m^2 \mu}{k} \tag{4-4}$$

The time delay is sensitive to the radial distance from the injection well and the hydraulic diffusivity and is not so sensitive to the injection rate. Thus, the transmission delay time can be revers to the hydraulic diffusivity of the aquifer. It can be used as a reference parameter to assess the hydraulic transmission capacity in the

aquifers.

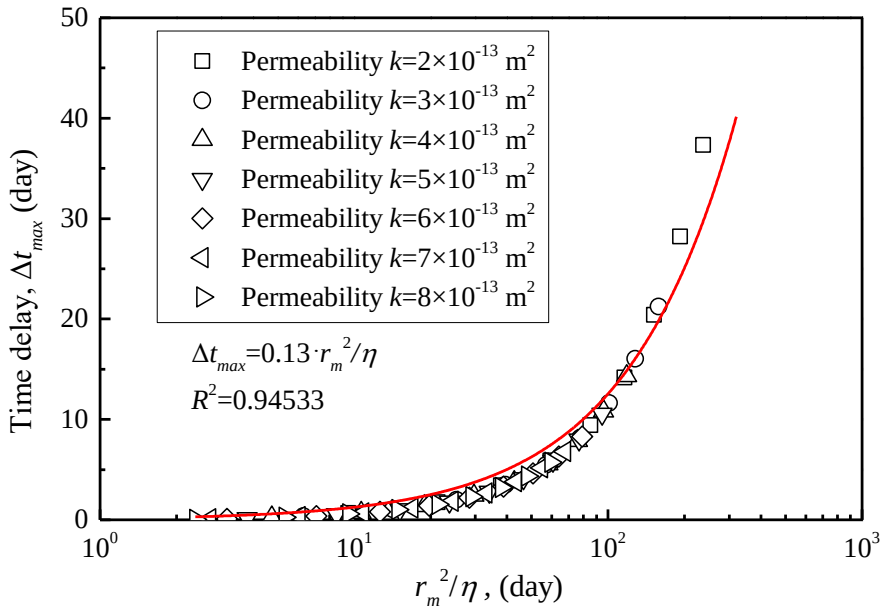

Figure 4-9. Time delay of observation well with r_m=1,000 m to 5,000 m in different permeability reservoir

It has been discussed in the above section, both the time delay Δt_{max} and the pressure fall-off time $t_{0.75}$-$t_{0.25}$ can be used as important parameters to evaluate the hydraulic diffusivity η of the aquifer. Figure 4-10 shows the numerical simulation results of the relationship between hydraulic diffusivity η and time ratio $\Delta t_{max}/(t_{0.75}$-$t_{0.25})$. Both time delay and fall-off time are inversely proportional to the hydraulic diffusivity, and the time ratio is also inversely proportional to hydraulic diffusivity. A rough magnitude of the time ratio in different hydraulic diffusivity aquifer was estimated. It is convenient to estimate the time delay of peak pressure using the time ratio when the fall-off time is measured. Because the fall-off time can help us to estimate the hydraulic diffusivity before an observation well is drilled. For example, in the case of r_m=3,000 m, Δt_{max} is equal to (0.4-0.7)×($t_{0.75}$-$t_{0.25}$) for η=2-4 m^2/s corresponding to the range of Tomakomai CCS project.

Besides, the estimating pressure ratio used in simulation studies can be revised by considering the time delay compared with the analytical equation. Therefore, the pressure ratio is proportional to the $\eta t/r_m^2$ should be revised as proportional to

$\eta(\Delta t_{max}+t_i)/r_m^2$. It can help us make a more accurate prediction of the pressure response in the observation well and estimate whether there is CO_2 leaking to the subsurface.

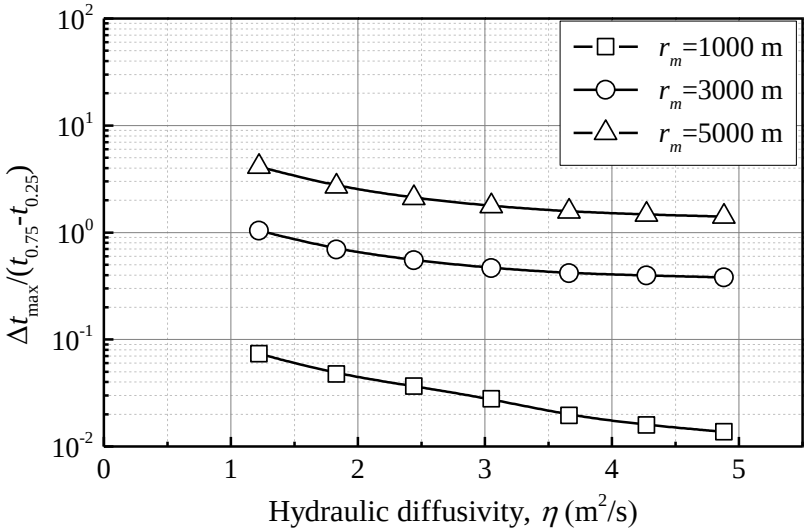

Figure 4-10. Numerical simulation results on time ratio against hydraulic diffusivity η (m^2/s)

4.4 Summary

This chapter summarizes the numerical simulation results of the pressure response in the observation well to the CO_2 injection with a single set of PBU and PFO. In particular, the pressure ratio R (= maximum response pressure at the observation well /PBU at the injection well) was obtained against the parameters such as horizontal permeability k_r, CO_2 mass injection rate q_m, and the location of the observation well, r_m. The conclusions are summarized below:

1 The value of R does not change significantly with q_m, but it decreases inversely proportion to r_m. For example, when r_m= 3 km, the range of the pressure ratio is estimated to be R= 0.07 to 0.12. A new variable was defined as the pressure ratio of pressure build-up and the corresponding pressure response in the observation well and the analytical solution was made to estimate the pressure ratio without considering the time delay Δt_{max}:

$$R=\frac{\Delta p_{\max}}{\Delta p}=(0.0425\text{-}0.06)\cdot\left(\ln\eta\frac{t_i}{r_m^{\,2}}+0.809\right)$$

2 The time delay Δt_{max}, which is the time difference between the shut-in time and the time that the maximum pressure response is recorded at the observation well, is also inversely proportional to η and increases in proportion to r_m^2. For instance, when the observation well distance is r_m=3 km, it was estimated Δt_{max}= 2 to 10 days.

Chapter 5: Influence of injection period and pattern

As the CCS project, the test CO_2 injection pattern in the early stage of the project performed a series of injections with multiple pressure build-ups and fall-offs, because CO_2 injection status was tested to check the pressure build-up against the injection rate in the early stage of CO_2 injection. An injection scheme case to investigate pressure response by the multiple CO_2 injections was assumed. The model includes six injection cycles with t_i=100 days injection period and 30 days shut-in based on the Tomakomai CCS project.

5.1 Effect of multiple-injection on CO_2 saturation distribution

As has been defined in Figure 2-8, the multiple-injection scheme includes 6 injection cycles. The CO_2 saturation results of cross-sectional on r, z axis of CO_2 saturation, at t=100 (End of injection cycle #1), 130, 230 (End of injection cycle # 2), and 260 days are shown in Figure 5-1. During the injection well was shut-in, the CO_2 plume diffuses at a slower speed, before a new cycle the CO_2 plume arrives at r_p=90 m. After another injection cycle, the CO_2 front moves to a new position from the injection well r_p=130 m.

Figure 5-2 shows the CO_2 saturation distribution of multiple-injection compared with the single injection at t_i=230 days (End of injection cycle # 2). Two injection periods have been performed for the multiple-injection scheme and the CO_2 plume arrives at r_p=130 m, while the CO_2 arrives at r_p=98 m for the single injection scheme. During the injection well is shut-in, the CO_2 plume diffuses very slow and moves only 14 m for the single injection scheme. For the multiple-injection scheme, after 30 days shut-in of injection well a new injection cycle speeds up the CO_2 plume diffuses speed, however, the diffuse speed is smaller than the first injection cycle because the radius of the CO_2 plume is larger with injection.

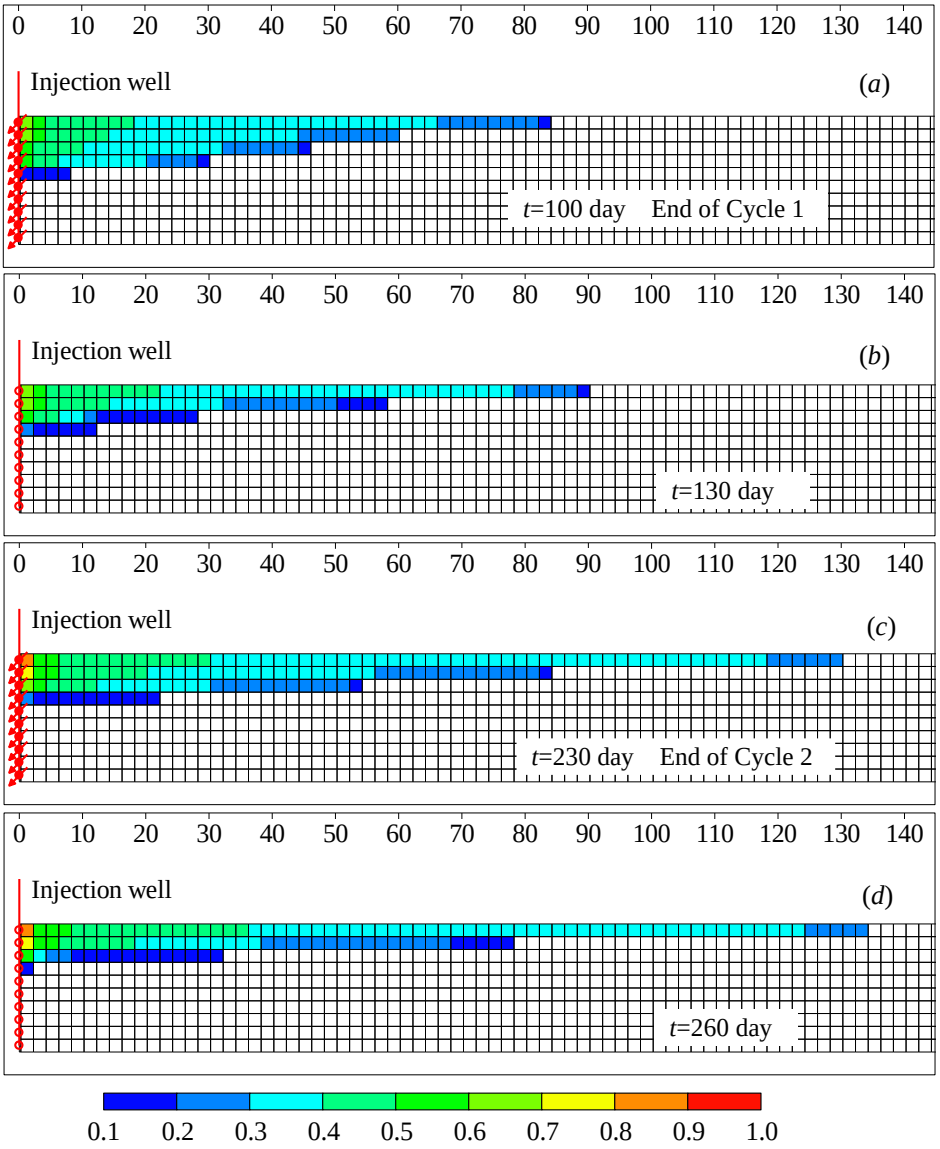

Figure 5-1. The CO_2 saturation front for injection cycle #1(Base case) and cycle #2 scheme vs. CO_2 saturation at different distances from the injection well

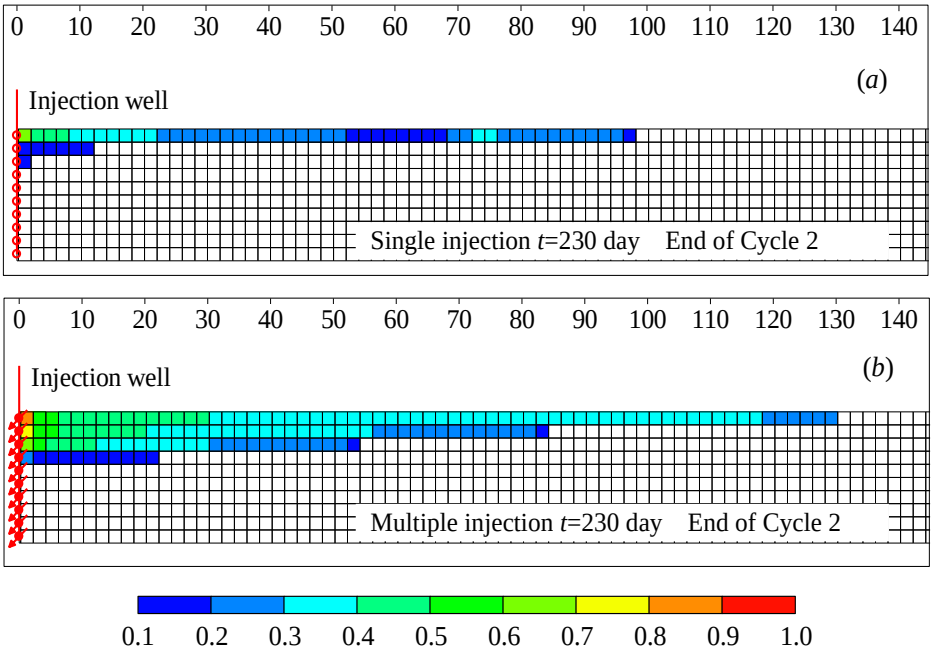

Figure 5-2. The CO_2 saturation pattern after two injections periods of multiple injections vs single injection

5.2 Effect of multiple build-ups and fall-offs on pressure response at the observation well

5.2.1 Effect of multiple injections on pressure build-ups and fall-offs at the injection well

The pressure build-up of the multiple-injection scheme at the injection well is shown in Figure 5-3. In the first injection cycle (the same as the base case), the reservoir fluid was only brine water, a pressure transient effect was observed. From cycle #2, the pressure build-up at the beginning of injection becomes gentle because there is already CO_2 in the vicinity of the injection well. The pressure build-up became smaller compared with the first injection cycle. The pressure build-up at the injection well shows a trend of slight dropping due to the changing CO_2 saturation and fluid viscosity around the injection well as discussed in the case of single build-up and fall-off case. So, the most dangerous period for the seal layer is at the beginning of CO_2

injection that high pressure is build-up in the bottom of the injection well.

After 30 days shut-in of the injection well, the pressure fell off to a smaller value, however, still larger than the initial pressure. From cycle #2, the pressure build-up both at the beginning and the end of a new injection cycle is smaller than the last injection cycle.

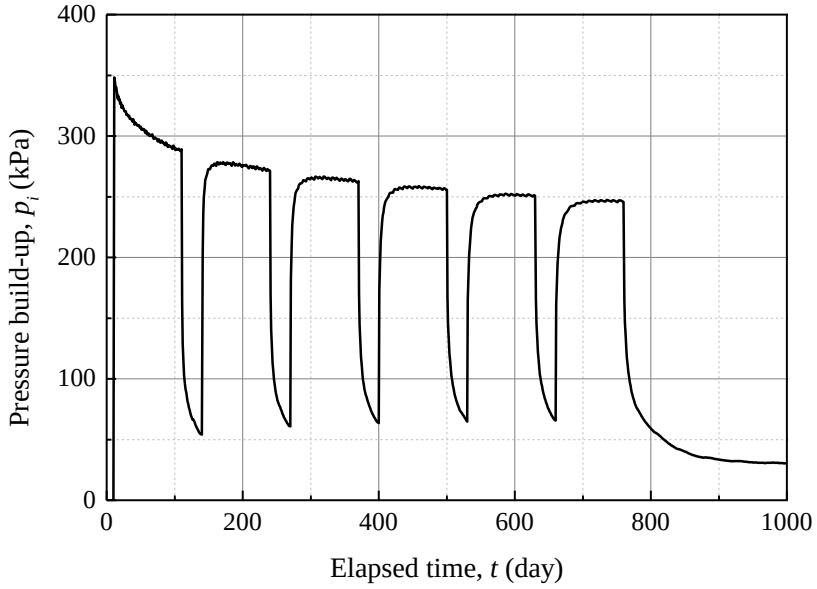

Figure 5-3 Numerical simulation results of pressure build-up at injection well for multiple-injection

5.2.2 Effect of multiple injections on pressure response

The simulation results of pressure response at the observation well located 3,000 m away from the injection well are shown in Figure 5-4. The CO_2 injection cycle #1 of the multiple-injection scheme is the same as the single injection case (base case) until the 2nd cycle starts.

It can be seen that each injection causes a pressure response peak at the observation well and drawdown in the injection well is similar to the pressure fall-off in the case of the single build-up and fall-off. The pressure build-up in each injection cycle is decreasing, while the pressure response Δp_{max} in each corresponding injection at the observation well is gradually increasing. The blue line shows the pressure ratio of

each injection cycle. It can be seen that the pressure ratio increases with the injection cycles and shows a tread to be a stable value. Because the reservoir tends to be a steady-state flow and the pressure value will be stable at the steady-state.

The delay time Δt_{max} does not show any difference between single and multiple injection scheme, this also shows the delay time reflects the hydraulic transmission capacity of the aquifer and it is inversely proportional to the hydraulic diffusivity.

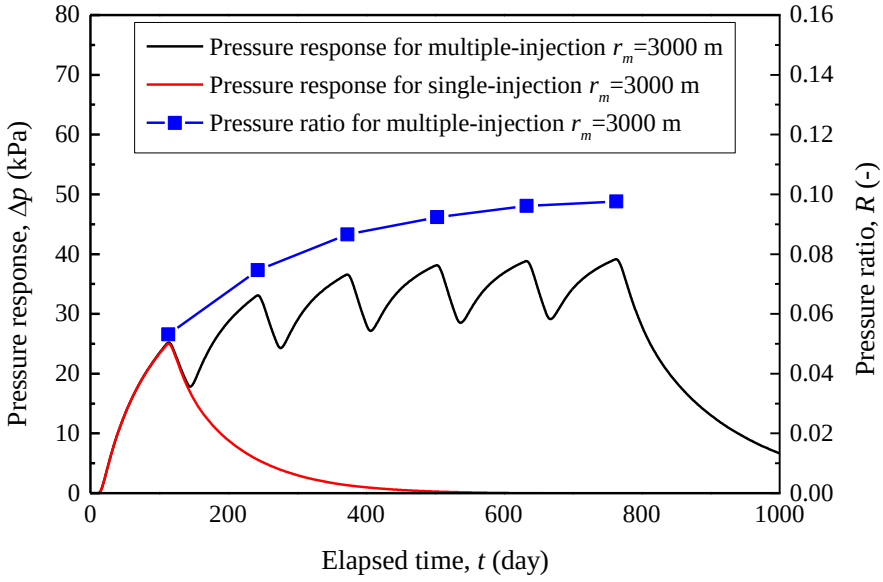

Figure 5-4. Pressure response and the pressure ratio of multiple injection scheme compared with single injection scheme in the observation well r_m=3000 m

Figure 5-5 shows the pressure response at the observation well of the distance r_m=3,000 m and the pressure ratio at different injection rates. The peak pressure value at the observation well is gradually increasing with injecting CO_2 into the reservoir, and the pressure turns to be a stable value which is similar to the pressure build-up at the single injection well. As the pressure build-up at the injection well turns to be a steady-state. The difference between the single injection and the multiple-injection becoming smaller. As is shown in Figure 5-4, the pressure build-up approximately to be 250 kPa and shows a smaller change with more injection cycles. On the other hand, the pressure response also reaches a relative peak value between different injection cycles. This result is shown in Figure 5-5 (*a*), pressure peak value in observation turns

to be a stable value.

The pressure ratio also approaches a stable value. The same tread was detected in different injection rates. This research focused on a short period injection mostly for the test CO_2 injection to design an observation well. For the normal injection operation, the pressure ratio should be analyzed by estimating the reservoir condition for the safety of the injected CO_2. A stable pressure value will be more convenient to determine a reliable pressure ratio by the simulation results.

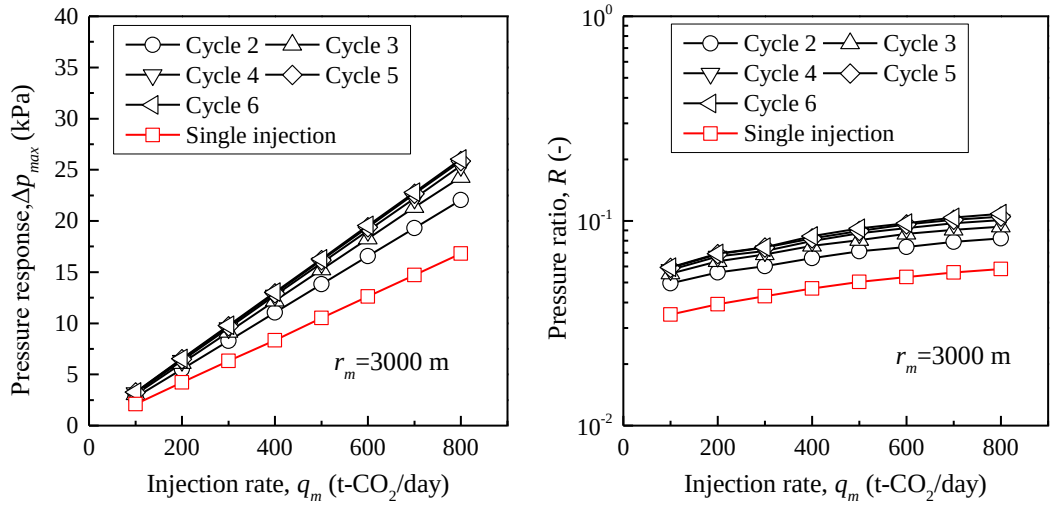

(*a*) (*b*)

Figure 5-5. Pressure response and pressure ratio R for r_m=3000 m of multiple injections compared with the single injection (base case) vs. injection rate; q_m (*a*) Pressure response (*b*) Pressure ratio R

5.3 Design of radial distance of an observation well

The observation well is drilled to observe the aquifer with CO_2 storage. Temperature and pressure gauges are installed in the bottom hole of the well for continuous monitoring of the aquifer. They are used to detect the CO_2 plume front development and verify that injected CO_2 is not leaked into shallower strata (Hannis et al., 2015; Metz et al., 2005). Most of the observation wells are used to monitor grasp the CO_2 plume front position (Hosseini et al., 2018; Hu et al., 2015; Mathieson et al., 2011; Mathieson et al., 2010). Normally it is drilled smaller than few hundreds of meters.

If the distance from the observation well to the injection well is too short, it can be used to detect pressure propagation. However, for a commercial CCS project, the drilled observation well has a possibility of making a leakage channel for stored CO_2. According to some *in situ* experience, the greatest risk of CO_2 leakage for any geological storage project is associated with old wells and observation wells (Mathieson et al., 2010).

In this section, an observation well that is planned to drill far from the injection well (>1000 m) is focused to discuss the distance from the injection well and the pressure sensor resolution.

Table 5-1. Resolution required for pressure measurement at the observation well (r_m=1000 m-5000 m p_i=1 MPa)

Radial distance r_m (m)	t_i=50 days		t_i=100 days	
	Pressure response Δp_{max} (kPa)	Spec. resolution (kPa)	Pressure response Δp_{max} (kPa)	Spec. resolution (kPa)
1000	144-156	5	190-200	5
2000	73-100	5	116-145	5
3000	41-70	1	76-112	1
4000	25-51	1	52-88	1
5000	18-38	1	36-70	1

Table 5-1 shows the simulation results of the pressure at the observation well range with different radial distances from the injection wel. For example, in the case of the observation well distance is equal to r_m=3 km, the minimum sensitivity of the pressure transmitter needs approximately 1 kPa order under the absolute pressure (or pressure resistance) of 10 to 11 MPa to obtain an accuracy of 2 digits. However, in the case of the minimum sensitivity is 10 kPa order, the well distance required should be lesser than 1 km.

The pressure build-up of the Tomakomai CCS project is about 450 kPa, and the

observation well OB-2 is drilled with a distance r_m=3,000 m from the injection well, according to the calculation, the maximum pressure value might be Δp_{max}=27 and 35 kPa is expected after 50 days and 100 days injection respectively. The specific resolution of the pressure transmitter installed in the observation well at r_m=3 km is required to be less than 1 kPa that is a tough specification under absolute pressure 10 to 11 MPa to analyze aquifer permeability characteristics. However, the differential pressure transmitter installed at OB-2 extends a pressure range of 200 kPa to 30,000 kPa which maybe not enough to detect the pressure response. A pressure transducer with a higher resolution needs to be installed.

5.4 Summary

In this chapter, an injection scheme of multiple CO_2 injections was analyzed and the design recommendations for the observation well located (>1000 m) from the injection well was proposed, the conclusions are summarized below:

1 The numerical simulation results of pressure ratio, R and the time delay, Δt_{max} for multiple schemes (6 sets of CO_2 injection with PBU and PFO), as shown in the initial stage of Tomakomai CCS, are compared with the single CO_2 injection scheme. It was revealed that R gradually increases with each repetition of multiple CO_2 injections, but Δt_{max} does not show any difference between single and multiple schemes.

2 When the pressure response at the observation well is used to estimate the aquifer condition based on the numerical simulation results, it was shown that the observation well location and the minimum sensitivity of the pressure transmitter installed in the well are important design factors for the observation well function. For example, in the case of the observation well distance is equal to r_m=3 km, the minimum sensitivity of the pressure transmitter needs approximately 1 kPa order under the absolute pressure (or pressure resistance) of 10 to 11 MPa to obtain an accuracy of 2 digits. However, in the case of the

minimum sensitivity is 10 kPa order, the well distance required should be lesser than, r_m= 1 km.

Chapter 6: Conclusions and outlook

6.1 Conclusions

The observation well has an important function to check the numerical simulation parameters to investigate CO_2 storage status in a deep saline aquifer, such as permeability, porosity, etc. affecting on pressure transient in the aquifer. In this numerical simulation study, pressure responses and their delay time at the observation well were investigated against a pressure build-up and fall-off at an injection well, because some injection tests are expected in an early stage of a CCS project to confirm CO_2 injectivity and pressure transient in the aquifer. Therefore, it is important to decide the location of the observation well and select a pressure transmitter with a reasonable resolution to measure the pressure response transmitted from the injector. Some sensitive study on the pressure response were also conducted The base model of the aquifer with 1000 m in depth, horizontal permeability k=370 md, porosity ϕ=30%, and open boundary at 10 km in radius was used for numerical simulations in considering the Tomakomai CCS project (Tomakomai CCS demonstration project). Results can be summarized as follows:

1 The pressure build-up p_i is proportional to the CO_2 injection rate q and reservoir fluid viscosity μ. During injecting CO_2, reservoir fluid viscosity μ is changing from water viscosity to CO_2 viscosity with the accumulate of injected CO_2. The BHP of injection well increases to a maximum value and drops instantly in a few hours from the beginning of injection. Then the BHP gradually tends to be flat and keeps a slight dropping rate. Steady-state flow equation can be used for a rough estimation of pressure build-up of injection well p_i for non-steady CO_2 pressure-time curve.

2 The CO_2 plume expansion radius of the top is r_p=84 m at t=100 day. The CO_2 plume front r_p expands almost proportionally to $t^{1/2}$ before $t<t_i$. After shut-in the injection well ($t>t_i$), the front is slowly expanding proportionally to $0.1t$ due

to the buoyancy force on the CO_2 plume. In addition. The CO_2 saturation around the injection well increases to about 0.35 with the elapsed time and reduces the effective fluid viscosity.

3 The increase in pressure build-up was inversely proportional to $k \cdot H$. However, the decrease in pressure build-up is about 5% compared to the case of salt water. It was the reason that the CO_2 saturation in the aquifer is limited by the irreducible water saturation of 0.65, and pressure build-up does not decrease significantly even if the CO_2 viscosity is less than 1/10 of water.

4 Compared with the field data of the Tomakomai CCS project, the pressure build-up and fall-off at the injection well were analyzed. The transmissivity of the Moebetsu Formation was estimated as 2.7×10^{-11} m^3 and the hydraulic diffusivity of the formstion is 2-4 m^2/s. So, assuming the permeability is k=1.35×10^{-11} to 2.7×10^{-11} m^2 (135 to 270 md) and the porosity is 0.2 to 0.4 of the Moebetsu Formation, the matrix rock compressibility of the Moebetsu Formation is estimated as C_r=0.14×10^{-9} to 1.11×10^{-6} Pa^{-1}. It was confirmed that the time required to reduce by half the pressure build-up decreases exponentially with increasing hydraulic diffusivity η.

5 The value of R does not change significantly with q_m, but it decreases in inverse proportion to r_m. For example, when r_m=3 km, the range of the pressure ratio is estimated to be R=0.07 to 0.12. A new variable was defined as the pressure ratio of pressure build-up and the corresponding pressure response in the observation well and the analytical solution was made to estimate the pressure ratio without considering the time delay $\Delta t_{\max}$:

$$R=\frac{\Delta p_{\max}}{\Delta p}=(0.0425\text{-}0.06)\cdot\left(\ln\eta\frac{t_i}{r_m^{\,2}}+0.809\right)$$

6 The time delay Δt_{max}, which is the time difference between the shut-in time and the time that the maximum pressure response is recorded at the observation well, is also inversely proportional to η and increases in proportion to r_m^2. For

instance, when the well distance is r_m=3 km, it was estimated Δt_{max}=2 to 10 days.

7 The numerical simulation results of pressure ratio, R and the time delay, Δt_{max} for multiple-injection scheme (6 sets of CO_2 injection with PBU and PFO), as shown in the initial stage of Tomakomai CCS project, are compared with the single CO_2 injection scheme. It was revealed that R gradually increases with each repetition of multiple CO_2 injections, but Δt_{max} does not show any difference between single and multiple schemes.

8 When the pressure response at the observation well is used to estimate the aquifer condition based on the numerical simulation results, it was shown that the observation well location and the minimum sensitivity of the pressure transmitter installed are important design factors for the observation well function. For example, in the case of the observation well distance is equal to r_m=3 km, the minimum sensitivity of the pressure transmitter needs approximately 1 kPa order under the absolute pressure (or pressure resistance) of 10 to 11 MPa to obtain an accuracy of 2 digits. However, in the case in the event in which the minimum sensitivity is 10 kPa order, the well distance required should be lesser than, r_m=1 km.

6.2 Outlook of future researches

1 This simulation study was carried by assuming a homogeneous aquifer, and the field data was limited. Some accurate geological model settings based on the field geological surveys need to be done. And a log of CO_2 injection operation needs to be considered to estimate the observation well pressure.

2 The influence of heterogeneity on pressure evolution needs further researches.

3 The estimation equation of pressure build-up is used by the steady-state equation. A more precise and widely used equation used the CO_2 viscosity need to be studied.

4 This simulation is assuming a constant pressure boundary condition. A bounded reservoir needs to be discussed for comparison.

Reference:

Alnes, H., Eiken, O., Nooner, S., Sasagawa, G., Stenvold, T., Zumberge, M., 2011. Results from Sleipner gravity monitoring: Updated density and temperature distribution of the CO_2 plume. Energy Procedia 4, 5504-5511.

Ashraf, M., 2014. Geological storage of CO_2: Heterogeneity impact on the behavior of pressure. International Journal of Greenhouse Gas Control 28, 356-368.

Benisch, K., Bauer, S., 2013. Short-and long-term regional pressure build-up during CO_2 injection and its applicability for site monitoring. International Journal of Greenhouse Gas Control 19, 220-233.

Cavanagh, A.J., Haszeldine, R.S., 2014. The Sleipner storage site: Capillary flow modeling of a layered CO_2 plume requires fractured shale barriers within the Utsira Formation. International Journal of Greenhouse Gas Control 21, 101-112.

Chadwick, R.A., Noy, D.J., Holloway, S., 2009. Flow processes and pressure evolution in aquifers during the injection of supercritical CO_2 as a greenhouse gas mitigation measure. Petrol Geosci 15, 59-73.

Cihan, A., Birkholzer, J.T., Zhou, Q., 2013. Pressure buildup and brine migration during CO_2 storage in multilayered aquifers. Groundwater 51, 252-267.

Cinar, Y., Bukhteeva, O., Neal, P.R., Allinson, W.G., Paterson, L., 2008. CO_2 storage in low permeability formations, SPE Symposium on Improved Oil Recovery. Society of Petroleum Engineers.

Costa, A., 2006. Permeability-porosity relationship: A reexamination of the Kozeny-Carman equation based on a fractal pore-space geometry assumption. Geophysical research letters 33.

Dake, L.P., 1983. Fundamentals of reservoir engineering. Elsevier.

Dietz, D., 1965. Determination of average reservoir pressure from build-up surveys. Journal of Petroleum Technology 17, 955-959.

Durucan, S., Shi, J.-Q., Sinayuc, C., Korre, A., 2011. In Salah CO_2 storage JIP: carbon dioxide plume extension around KB-502 well–new insights into reservoir behaviour at the In Salah storage site. Energy Procedia 4, 3379-3385.

Edenhofer, O., Seyboth, K., 2013. Intergovernmental panel on climate change (IPCC).

Ehlig-Economides, C.A., Anchliya, A., Song, B., 2010. Pressure fall-off method for CO_2 leakage detection in deep saline aquifers, SPE EUROPEC/EAGE Annual Conference and Exhibition. Society of Petroleum Engineers.

Eiken, O., Ringrose, P., Hermanrud, C., Nazarian, B., Torp, T.A., Høier, L., 2011. Lessons learned from 14 years of CCS operations: Sleipner, In Salah and Snøhvit. Energy Procedia 4, 5541-5548.

Escobar, F.H., Montealegre-M, M., 2008. Determination of horizontal permeability from the elliptical flow of horizontal wells using conventional analysis. J. Pet. Sci. Eng. 61, 15-20.

Finley, R.J., Frailey, S.M., Leetaru, H.E., Senel, O., Couëslan, M.L., Scott, M., 2013. Early operational experience at a one-million tonne CCS demonstration project, Decatur, Illinois, USA. Energy Procedia 37, 6149-6155.

Fitts, J.P., Peters, C.A., 2013. Caprock fracture dissolution and CO_2 leakage. Reviews in Mineralogy and Geochemistry 77, 459-479.

Fujita, C., Hiratsuka, Y., Yamamoto, H., Nakajima, T., Xue, Z., 2017. Numerical simulation study on mitigation of the pressure build-up in the geological formation during injection of CO_2. Energy Procedia 114, 4765-4774.

Furre, A.-K., Kiær, A., Eiken, O., 2015. CO_2-induced seismic time shifts at Sleipner. Interpretation 3, SS23-SS35.

Gao, S., Wei, N., Li, X., Wang, Y., Wang, Q., 2014. Cap rock CO_2 breakthrough pressure measurement apparatus and application in Shenhua CCS project. Energy Procedia 63, 4766-4772.

Garimella, S., Ahmed, S., Hossain, M., 2019. Comparison of different models for predicting drainage relative permeability using pore scale numerical simulation of supercritical carbon dioxide and brine flow, IOP Conference Series: Materials Science and Engineering. IOP Publishing 495, 012111.

Gasda, S.E., Wangen, M., Bjørnarå, T.I., Elenius, M.T., 2017. Investigation of caprock integrity due to pressure build-up during high-volume injection into the Utsira formation. Energy Procedia 114, 3157-3166.

Gaus, I., Azaroual, M., Czernichowski-Lauriol, I., 2005. Reactive transport modelling of the impact of CO_2 injection on the clayey cap rock at Sleipner (North Sea). Chem Geol 217, 319-337.

Goel, M., 2012. Sustainable energy through carbon capture and storage: role of geo-modeling studies. Energy & environment 23, 299-317.

Goertz-Allmann, B.P., Kühn, D., Oye, V., Bohloli, B., Aker, E., 2014. Combining microseismic and geomechanical observations to interpret storage integrity at the In Salah CCS site. Geophysical Journal International 198, 447-461.

Grude, S., Landrø, M., Dvorkin, J., 2014. Pressure effects caused by CO_2 injection in the Tubåen Fm., the Snøhvit field. International Journal of Greenhouse Gas Control 27, 178-187.

Hannis, S., Chadwick, A., Pearce, J., Jones, D., White, J., Wright, I., Connelly, D., Widdicombe, S., Blackford, J., White, P., 2015. Review of offshore monitoring for CCS Projects, 2015/02, July, 2015.

Hansen, O., Gilding, D., Nazarian, B., Osdal, B., Ringrose, P., Kristoffersen, J.-B.,

Eiken, O., Hansen, H., 2013. Snøhvit: The history of injecting and storing 1 Mt CO_2 in the fluvial Tubåen Fm. Energy Procedia 37, 3565-3573.

Heath, J.E., McKenna, S.A., Dewers, T.A., Roach, J.D., Kobos, P.H., 2014. Multiwell CO_2 injectivity: impact of boundary conditions and brine extraction on geologic CO_2 storage efficiency and pressure buildup. Environmental science & technology 48, 1067-1074.

Hosseini, S.A., Shakiba, M., Sun, A., Hovorka, S., 2018. In-zone and above-zone pressure monitoring methods for CO_2 geologic storage. Geological Carbon Storage: Subsurface Seals and Caprock Integrity, 225-241.

Hu, L., Bayer, P., Alt-Epping, P., Tatomir, A., Sauter, M., Brauchler, R., 2015. Time-lapse pressure tomography for characterizing CO_2 plume evolution in a deep saline aquifer. International Journal of Greenhouse Gas Control 39, 91-106.

Hubbert, M.K., 1953. Entrapment of petroleum under hydrodynamic conditions. Aapg Bulletin 37, 1954-2026.

Hubbert, M.K., Willis, D.G., 1972. Mechanics of hydraulic fracturing.

Humlum, O., Stordahl, K., Solheim, J.-E., 2013. The phase relation between atmospheric carbon dioxide and global temperature. Global and Planetary Change 100, 51-69.

IEACHG, 2010. Injection strategies for CO_2 storage sites. IEA Greenhouse Gas R&D Programme (IEAGHG), Australia.

Japan CCS CO., L., 2016-2020. Tomakomai CCS Demostration Project, http://www.jccs-tomakomai-monitoring.com/JCCS/index.php/top_e/.

Joshi, A., Gangadharan, S., Leonenko, Y., 2016. Modeling of pressure evolution during multiple well injection of CO_2 in saline aquifers. Journal of Natural Gas

Science and Engineering 36, 1070-1079.

Kazemi, H., Merrill, L., Jargon, J., 1972. Problems in interpretation of pressure fall-off tests in reservoirs with and without fluid banks. Journal of Petroleum Technology 24, 1,147-141,156.

Kelley, M., Abbaszadeh, M., Mishra, S., Mawalkar, S., Place, M., Gupta, N., Pardini, R., 2014. Reservoir characterization from pressure monitoring during CO_2 injection into a depleted pinnacle reef–MRCSP commercial-scale CCS demonstration project. Energy Procedia 63, 4937-4964.

Khan, S., Khulief, Y., Al-Shuhail, A., 2020. Effects of reservoir size and boundary conditions on pore-pressure buildup and fault reactivation during CO_2 injection in deep geological reservoirs. Environ. Earth Sci. 79, 1-23.

Kim, K.-Y., Han, W.S., Kim, T., 2011. Numerical study of pressure evolution from CO_2 injection in saline aquifers. Energy Procedia 4, 4532-4537.

Kim, M., Shin, H., 2019. Application of a dual tubing CO_2 injection-water production horizontal well pattern for improving the CO_2 storage capacity and reducing the CAPEX: A case study in Pohang basin, Korea. International Journal of Greenhouse Gas Control 90, 102813.

Kweku, D.W., Bismark, O., Maxwell, A., Desmond, K.A., Danso, K.B., Oti-Mensah, E.A., Quachie, A.T., Adormaa, B.B., 2017. Greenhouse effect: greenhouse gases and their impact on global warming. Journal of Scientific research and reports, 1-9.

Lake, J.A., Lomax, B.H., 2019. Plant responses to simulated carbon capture and storage (CCS) CO_2 pipeline leakage: the effect of soil type. Greenhouse Gases: Science and Technology 9, 397-408.

Ledley, T.S., Sundquist, E.T., Schwartz, S.E., Hall, D.K., Fellows, J.D., Killeen, T.L., 1999. Climate change and greenhouse gases. Eos, Transactions American

Geophysical Union 80, 453-458.

Liebscher, A., Möller, F., Bannach, A., Köhler, S., Wiebach, J., Schmidt-Hattenberger, C., Weiner, M., Pretschner, C., Ebert, K., Zemke, J., 2013. Injection operation and operational pressure–temperature monitoring at the CO_2 storage pilot site Ketzin, Germany—Design, results, recommendations. International Journal of Greenhouse Gas Control 15, 163-173.

Mathias, S.A., de Miguel, G.J.G.M., Thatcher, K.E., Zimmerman, R.W., 2011. Pressure buildup during CO_2 injection into a closed brine aquifer. Transport in porous media 89, 383-397.

Mathias, S.A., Hardisty, P.E., Trudell, M.R., Zimmerman, R.W., 2009a. Approximate solutions for pressure buildup during CO_2 injection in brine aquifers. Transport in Porous Media 79, 265-284.

Mathias, S.A., Hardisty, P.E., Trudell, M.R., Zimmerman, R.W., 2009b. Screening and selection of sites for CO_2 sequestration based on pressure buildup. International Journal of Greenhouse gas control 3, 577-585.

Mathieson, A., Midgely, J., Wright, I., Saoula, N., Ringrose, P., 2011. In Salah CO_2 Storage JIP: CO_2 sequestration monitoring and verification technologies applied at Krechba, Algeria. Energy Procedia 4, 3596-3603.

Mathieson, A., Midgley, J., Dodds, K., Wright, I., Ringrose, P., Saoul, N., 2010. CO_2 sequestration monitoring and verification technologies applied at Krechba, Algeria. The Leading Edge 29, 216-222.

Matthews, C.S., Russell, D.G., 1967. Pressure buildup and flow tests in wells. Henry L. Doherty Memorial Fund of AIME.

Meckel, T.A., Zeidouni, M., Hovorka, S.D., Hosseini, S.A., 2013. Assessing sensitivity to well leakage from three years of continuous reservoir pressure

monitoring during CO_2 injection at Cranfield, MS, USA. International Journal of Greenhouse Gas Control 18, 439-448.

Metz, B., Davidson, O., De Coninck, H., Loos, M., Meyer, L., 2005. IPCC special report on carbon dioxide capture and storage. Prepared by Working Group III of the Intergovernmental Panel on Climate Change. IPCC, Cambridge University Press: Cambridge, United Kingdom and New York, USA 4.

Mikhaylov, A., Moiseev, N., Aleshin, K., Burkhardt, T., 2020. Global climate change and greenhouse effect. Entrepreneurship and Sustainability Issues 7, 2897.

Nordbotten, J.M., Celia, M.A., Bachu, S., 2005. Injection and storage of CO_2 in deep saline aquifers: Analytical solution for CO_2 plume evolution during injection. Transport in Porous Media 58, 339-360.

Obergassel, W., Arens, C., Hermwille, L., Kreibich, N., Mersmann, F., Ott, H., Wand-Helmreich, H., 2018. The calm before the storm: An assessment of the 23rd Climate Change Conference COP23 in Bonn. Wuppertal Institute 11.

Oruganti, Y., Bryant, S.L., 2009. Pressure build-up during CO_2 storage in partially confined aquifers. Energy Procedia 1, 3315-3322.

Otake, M., 2013. Evaluation of CO_2 underground behavior from injector's time-lapse pressure fall off analysis: a case study of CO_2 aquifer storage project. Energy Procedia 37, 3307-3318.

Paul, A., Laurila, T., Vuorinen, V., Divinski, S.V., 2014. Thermodynamics, diffusion and the Kirkendall effect in solids. Springer.

Pourtoy, D., Onaisi, A., Lescanne, M., Thibeau, S., Viaud, C., 2013. Seal Integrity of the Rousse depleted gas field impacted by CO_2 injection (Lacq industrial CCS reference project France). Energy Procedia 37, 5480-5493.

Prevedel, B., Martens, S., Norden, B., Henninges, J., Freifeld, B.M., 2014. Drilling

and abandonment preparation of CO_2 storage wells–Experience from the Ketzin pilot site. Energy Procedia 63, 6067-6078.

Qiao, H., Zheng, F., Jiang, H., Dong, K., 2019. The greenhouse effect of the agriculture-economic growth-renewable energy nexus: evidence from G20 countries. Sci Total Environ 671, 722-731.

Rahman, F.A., Aziz, M.M.A., Saidur, R., Bakar, W.A.W.A., Hainin, M., Putrajaya, R., Hassan, N.A., 2017. Pollution to solution: Capture and sequestration of carbon dioxide (CO_2) and its utilization as a renewable energy source for a sustainable future. Renewable and Sustainable Energy Reviews 71, 112-126.

Ringrose, P., Sæther, Ø., Equinor, A., 2020. Injection operations: Insights from Sleipner and Snøhvit.

Ritchie, H., Roser, M., 2020. CO_2 and greenhouse gas emissions. Our world in data.

Romasheva, N., Ilinova, A., 2019. CCS projects: How regulatory framework influences their deployment. Resources 8, 181.

Rutqvist, J., 2012. The geomechanics of CO_2 Storage in deep sedimentary formations. Geotechnical and Geological Engineering 30, 525-551.

Rutqvist, J., Vasco, D.W., Myer, L., 2010. Coupled reservoir-geomechanical analysis of CO_2 injection and ground deformations at In Salah, Algeria. International Journal of Greenhouse Gas Control 4, 225-230.

Sato, K., Horne, R.N., 2018. Time-lapse analysis of pressure transients due to ocean tides for estimating CO_2 saturation changes. International Journal of Greenhouse Gas Control 78, 160-167.

Sawada, Y., Tanaka, J., Suzuki, C., Tanase, D., Tanaka, Y., 2018. Tomakomai CCS Demonstration Project of Japan, CO_2 Injection in Progress. Energy Procedia 154, 3-8.

Shackley, S., McLachlan, C., Gough, C., 2005. The public perception of carbon dioxide capture and storage in the UK: results from focus groups and a survey. Climate Policy 4, 377-398.

Shukla, R., Ranjith, P., Haque, A., Choi, X., 2010. A review of studies on CO_2 sequestration and caprock integrity. Fuel 89, 2651-2664.

Singh, H., 2018. Impact of four different CO_2 injection schemes on extent of reservoir pressure and saturation. Advances in Geo-Energy Research 2, 305-318.

Smith, D., Noy, D., Holloway, S., Chadwick, R., 2011. The impact of boundary conditions on CO_2 storage capacity estimation in aquifers. Energy Procedia 4, 4828-4834.

Stork, A.L., Verdon, J.P., Kendall, J.-M., 2015. The microseismic response at the In Salah Carbon Capture and Storage (CCS) site. International Journal of Greenhouse Gas Control 32, 159-171.

Szulczewski, M.L., 2013. The subsurface fluid mechanics of geologic carbon dioxide storage. Massachusetts Institute of Technology.

Tanaka, Y., Abe, M., Sawada, Y., Tanase, D., Ito, T., Kasukawa, T., 2014. Tomakomai CCS Demonstration Project in Japan, 2014 Update. 12th International Conference on Greenhouse Gas Control Technologies, Ghgt-12 63, 6111-6119.

Tanaka, Y., Sawada, Y., Tanase, D., Tanaka, J., Shiomi, S., Kasukawa, T., 2017. Tomakomai CCS Demonstration Project of Japan, CO_2 injection in process. Energy Procedia 114, 5836-5846.

Tao, Q., Bryant, S.L., Meckel, T., 2013. Modeling above-zone measurements of pressure and temperature for monitoring CCS sites. International Journal of Greenhouse Gas Control 18, 523-530.

Terry, R.E., Rogers, J.B., Craft, B.C., 2015. Applied petroleum reservoir engineering.

Pearson Education.

Thibeau, S., Bachu, S., Birkholzer, J., Holloway, S., Neele, F., Zhou, Q., 2014. Using pressure and volumetric approaches to estimate CO_2 storage capacity in deep saline aquifers. Energy Procedia 63, 5294-5304.

Van Everdingen, A., Hurst, W., 1949. The application of the Laplace transformation to flow problems in reservoirs. Journal of Petroleum Technology 1, 305-324.

Verdon, J.P., Kendall, J.M., Stork, A.L., Chadwick, R.A., White, D.J., Bissell, R.C., 2013. Comparison of geomechanical deformation induced by megatonne-scale CO_2 storage at Sleipner, Weyburn, and In Salah. Proceedings of the National Academy of Sciences of the United States of America 110, E2762-E2771.

Vilarrasa, V., Bolster, D., Dentz, M., Olivella, S., Carrera, J., 2010. Effects of CO_2 compressibility on CO_2 storage in deep saline aquifers. Transport in porous media 85, 619-639.

Wiese, B., Zimmer, M., Nowak, M., Pellizzari, L., Pilz, P., 2013. Well-based hydraulic and geochemical monitoring of the above zone of the CO_2 reservoir at Ketzin, Germany. Environ. Earth Sci. 70, 3709-3726.

Wu, H., Bai, B., Li, X., 2018. An advanced analytical solution for pressure build-up during CO_2 injection into infinite saline aquifers: The role of compressibility. Adv Water Resour 112, 95-105.

Wu, H., Bai, B., Li, X., Gao, S., Liu, M., Wang, L., 2016. An explicit integral solution for pressure build-up during CO_2 injection into infinite saline aquifers. Greenhouse Gases: Science and Technology 6, 633-647.

Yang, F., Bai, B.J., Tang, D.Z., Dunn-Norman, S., Wronkiewicz, D., 2010. Characteristics of CO_2 sequestration in saline aquifers. Petrol Sci 7, 83-92.

Zhang, K., Xie, J., Li, C., Hu, L., Wu, X., Wang, Y., 2016a. A full chain CCS demonstration project in northeast Ordos Basin, China: operational experience and challenges. International Journal of Greenhouse Gas Control 50, 218-230.

Zhang, L., Dilmore, R.M., Bromhal, G.S., 2016b. Effect of outer boundary condition, reservoir size, and CO_2 effective permeability on pressure and CO_2 saturation predictions under carbon sequestration conditions. Greenhouse Gases: Science and Technology 6, 546-560.

Zhang, Z.H., Huisingh, D., 2017. Carbon dioxide storage schemes: Technology, assessment and deployment. Journal of Cleaner Production 142, 1055-1064.

Zhong, Z., Sun, A.Y., Yang, Q., Ouyang, Q., 2019. A deep learning approach to anomaly detection in geological carbon sequestration sites using pressure measurements. Journal of hydrology 573, 885-894.

Zhou, Q., Birkholzer, J.T., 2011. On scale and magnitude of pressure build-up induced by large-scale geologic storage of CO_2. Greenhouse Gases: Science and Technology 1, 11-20.